p-ISSN : 2335-1357 e-ISSN : 2437-1122

Mediterranean Journal of Modeling and Simulation

Med. J. Model. Simul. 05 (2016) 001-016

Application of Cat Swarm Optimization in testing Static Load Models for Voltage Stability

G. Naveen Kumar [a] *

[a] Department of EEE, VNR VJIET, Hyderabad, India

ARTICLE INFO

Article history :
Received November 2015
Accepted February 2016

Keywords :
Continuation Power Flow ;
Cat Swarm Optimization ;
Static Load Models ;
Unified Power Flow Controller ;
Voltage Stability.

ABSTRACT

Power System Load Modeling is a method which is used to model the power system and essential for voltage stability studies. Voltage stability defines the ability of a power network to maintain steady state voltages at all the buses under normal operating conditions, and when subjected to a disturbance. The research presented as part of this paper, deals with analysis of different static load models for voltage stability studies. The precision of the results are directly related to the load models used in this analysis. The method is analyzed using continuation power flow routine. Flexible AC Transmission System technology with a combination of Cat Swarm Optimization Meta Heuristic Search approach is applied to give a solution for the problem of instability. The effectiveness of the proposed method is demonstrated through quantitative simulation on standard IEEE 14 bus system for contingency condition.

1. Introduction

During the system disturbances and their impacts on other power system elements, system stability is imperilled. The probability of moving to the global instability increases. This will usually make a power system to break up in the isolated sub-systems known as islands and then a complete blackout results unless some precautions are considered. Voltage Stability or Load Stability is one of the concerns in power systems which are heavily loaded, faulted or having a shortage of reactive power [14, 15]. The problem of voltage stability concerns the whole power system, although it usually has a large involvement in one critical area of the power system. Example case of recent massive black out in India's power grid happens to the worst in the decade. Three out of the five regional power grids collapsed leaving about six hundred and seventy million people powerless making July 2012 as the largest blackout month in history. According to [2, 13] Power System Load Modeling is a technique used to model the power system and essential for stability assessments. In this paper, we are trying to analyze different static

*Email : gutha26@gmail.com

load models for voltage stability studies. The accuracy and correctness of the results for voltage stability are directly related to the load models used in this analysis. Different load models would greatly affect voltage stability aspect of an interconnected power system. We are using continuation power flow to analyze the effects of different load models and compare the results.

Flexible AC Transmission Systems in short FACTS controllers are used to control the variables such as phase angle and voltage magnitude at a given bus and line impedance where a voltage collapse is observed [16, 4]. Introducing FACTS controllers is the most effective way for utilities to improve the voltage profile and voltage stability margin of the system. As the size and the cost of the FACTS devices are high, an optimal location and size has to be identified before they are actually installed [8, 9].

Introducing FACTS in stability issues is not a new topic and is being studied over many long years. But the introducing them while analyzing different static load models when the system is under a contingent condition, a generator outage that directly has its effect felt on load centers is a new topic discussed in this paper.

2. Problem formulation

Accurate modeling of loads continues to be a difficult task due to several reasons. Lack of precise information on the composition of the load, changing of load composition with time like day and week, seasons, weather, through time and more influence the load models. Electric utility analysts and their management need evidence of the benefits in improved load representation to justify the effort and expense of collecting and processing load data. Also to modify computer program load models. The interest in load modeling has increased in the last few years, and power system load modeling has become a new research area in power systems stability. Several studies have reported the critical effect of load representation in voltage stability studies. This leads to identify accurate load models than the traditionally used ones.

Though ours is not the first paper to test various static load models for determining the voltage stability limits of a power network, it happens to be the first one to analyze four different static load models under one roof and also to apply cat swarm optimization technique for the power networks under contingent conditions. The static load models we are testing include ZIP model or Polynomial model, Exponential Load Model, Frequency Dependent load model and Voltage Dependent load model. FACTS technology is employed to give a solution for instability margins.

To analyze the maximum loading parameter and bus voltage magnitude profile aspects, we are simulating the PV curves for the system with different types of loads. We are trying to analyze these loads under contingency condition which was not addressed earlier. We are considering the problem case of generator outage contingency while performing the load testing. We are trying to improve the voltage magnitude profile, maximum loading parameter using FACTS controllers. A solution is given to mitigate the harmful effects of voltage instability criterion on the power system using FACTS controllers via Cat Swarm Optimization. The objective function for achieving the above is defined as follows

$$F = \{F_1, F_2, F_3\} \tag{1}$$

The functions F_1, F_2 and F_3 are defined and used in optimization process.

$$F = \Phi_1 F_1 + \Phi_2 F_2 + \Phi_3 F_3 \tag{2}$$

In our study, the fitness function is defined as a sum of three terms with individual criteria. The first part of the objective function concerns the voltage level. It is favorable that buses voltages be as close as possible to 1 p.u. Equation (3) shows the voltage deviation in all buses.

$$F_1 = F_V = \sum_{i=1}^{nb} (V_i)^2 \tag{3}$$

Where nb is the number of buses and V_i is the voltage of bus i.

F_2-This function represents the optimal location and size of UPFC which has its dependence on F_1.This is related to having the minimum possible UPFC sizes regarding to the control of UPFC that is given by (4).

$$F_2 = F_s = \alpha \sum_{j=1}^{m} Q_j \tag{4}$$

Where 'm' is the number of UPFC and 'Q_j' is the value of UPFC's Kvar and 'α' is a weight in order that the terms in the fitness function are comparable in magnitude. Value of UPFC's Kvar considering the control strategy and UPFC's model is achieved. The maximum loadability of power system is extremely important and hence it is considered as the third part of the objective function. So, finally, the third issue in our problem is determining inverse of maximum loadability, given as follows :

$$F_3 = F_{SM} = 1/\lambda_{Critical} \tag{5}$$

Therefore, the objective function is given by the following equation.

$$F = \Phi_1 F_V + \Phi_2 F_S + \Phi_3 F_{SM} \tag{6}$$

The objective function for the load model testing is defined as follows.

$$E = \{E_1, E_2\} \tag{7}$$

The functions E_1 and E_2 are defined as

The first part of the objective function concerns the voltage level. It is favorable that buses voltages be as close as possible to 1 per unit according to equation (8).

$$E_1 = E_V = \sum_{i=1}^{nb} (V_i)^2 \tag{8}$$

The second issue in our problem is determining inverse of maximum loadability, given as follows.

$$E_3 = E_{SM} = 1/\lambda_{Critical} \tag{9}$$

The functions E_1 and E_2 are defined and used in optimization process.

$$E = \mu_1 E_1 + \mu_2 E_2 \tag{10}$$

Therefore, the objective function is given by (11).

$$E = \mu_1 E_V + \mu_2 E_{SM} \tag{11}$$

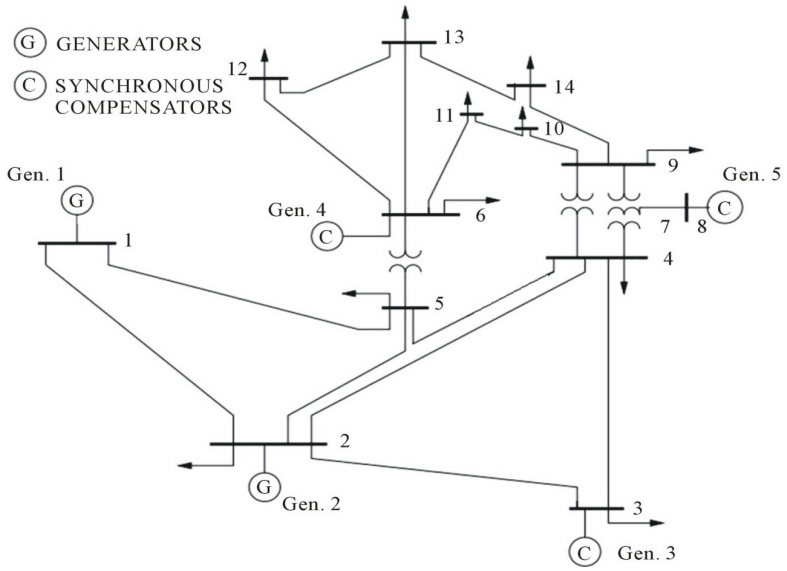

Fig. 1 – IEEE 14 Bus Network.

3. Cat swarm optimization, facts and static load models

3.1. Introduction to Cat Swarm Optimization

Optimization techniques find a variety of use in many fields. The use of these techniques in power systems is playing an important role for the optimal location of FACTS devices. In the field of optimization, many algorithms were being proposed in the recent past.

To name a few, Genetic Algorithm (GA), Ant Colony Optimization (ACO), Particle Swarm Optimization (PSO), Simulated Annealing (SA) etc. Some of these optimization algorithms were developed based on swarm intelligence. Cat Swarm Optimization in short CSO, the algorithm, is motivated from PSO and ACO. According to the literatures, PSO with weighting factor usually finds the better solution faster than the pure PSO, but according to the experimental results, Cat Swarm Optimization (CSO) presents even much better performance [10, 11]. CSO is a Meta Heuristic search approach. This search technique is considered to be a very simple one as compared to other optimization and heuristic approaches existing such as GA, SA, CCEA, PSO etc. to name a few. We can though use a simple local search algorithm like a gradient based optimization for optimal location of FACTS controllers but when applied to large interconnected power networks, it fails in identifying accurate solution and is not a suggested approach. Also the procedures like GA, PSO, ACO, SA etc. become very tedious to implement and are already tested by many researchers and have reached a saturation level. One can appreciate the importance of Cat Swarm optimization which was presented in articles [1] and [3]. Authors have stressed the point in using this algorithm, an advanced one which combines speed and ease in finding solution, an optimum one for various problems of engineering.

In Cat Swarm Optimization, we first model the behavior of cats into two sub-models, namely, seeking mode and tracing mode. Seeking mode is used to model the situation of the cat, which is resting, looking around and seeking the next position to move to. Tracing mode is the sub-model for modeling the case of the cat in tracing some targets. Once a cat goes into tracing mode, it moves according to its own velocities for every dimension [12]. The algorithmic flow routine for the CSO can be explained through the flow chart in Fig. 2 taken from [11].

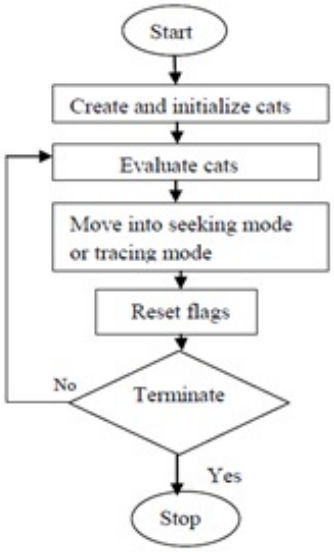

Fig. 2 – Flow chart for Cat Swarm Optimization.

3.2. FACTS Controllers

Flexible AC Transmission Systems (FACTS) are being used in power systems since 1970s with an objective of improving system dynamic performance [5]. Due to the environmental, right of way, and cost problems in power systems, many transmission lines have been forced to operate at almost their full capacities worldwide. FACTS controllers enhance the static performance which includes increased loading, congestion management, reduced system loss, economic operation, etc., and dynamic performance that is damping of power system oscillation, increased stability limits, etc. The concept of FACTS involves family of semiconductor and electronic devices, with advanced and reliable controls. We are using Unified Power Flow Controller in our application.

3.2.1. Unified Power Flow Controller

The Unified Power Flow Controller, in short, UPFC comes with a combination of a static synchronous compensator (STATCOM) and static synchronous series compensator (SSSC) coupled with a common DC voltage link. The main advantage of the UPFC is in controlling active and reactive power flows in a transmission line. The connection structure is shown in figure 3.

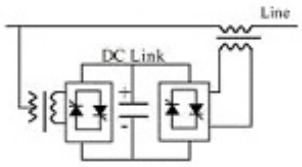

Fig. 3 – Structure of UPFC.

3.3. Static Load Models Used

3.3.1. ZIP model or polynomial model

The static characteristics of the load can be classified into constant impedance, constant current and constant power load, depending on the power relation to the voltage. Constant impedance loads examples : Residential loads and lighting loads such as bulbs e.t.c. Constant current load examples : Transistors, transducers and incandescent lamps. Constant power loads are switching regulators and industrial loads.

3.3.2. Frequency Dependent model

A static load model which includes frequency dependence is called a frequency dependent load. Examples for frequency dependent loads are refrigerators, freezers, air conditioners, water heaters, pumps and ovens.

3.3.3. Voltage Dependent model

A voltage dependent load is an electrical device whose power consumption changes with the voltage being supplied to it. Examples for these loads are the most common types of incandescent lamps, standard tungsten filament lamps, tungsten halogen and reflector lamps and motor load.

3.3.4. Exponential recovery model

In exponential load model the active and reactive power injections of load bus are related to bus voltage through exponential function. Examples for these loads are residential loads, lighting loads and motor loads.

4. Implementation, results and discussion

We are installing and simulating the IEEE 14 bus system independently with each type of the load models described in section 4.3 at the load buses. The system modeled and loaded with these different static loads will become instable. The values of the voltage magnitude profiles at different buses are depicted in table 1. The maximum loading parameter details with and without loads are given in Table 2. From the results in tables 1 and 2, we can observe that frequency dependent loads and exponential recovery loads have a considerable increase in loading parameter when compared to ZIP and voltage dependent loads. Even though the maximum loading parameter is appreciable, the voltages magnitude profiles at different buses were observed to be less. This is not around 1P.U. Apart from the above, we have also performed generator outage contingency. There are four working generators in the case study and contingency is performed for all the four generators. The results for n-1 generator outage contingency are given in Table 3. Generator6 contingency was observed to be the worst case. For the different types of load models tested, generator6 contingency is performed and the results of voltage profile are taken.

Table 1 – Voltages Magnitude Profiles for different loads.

BUS. No.	ZIP load	Voltage Dependant Load	Frequency Dependant Load	Exponential Recovery Load
Bus1	1.0566	1.0566	1.0566	1.0566
Bus2	0.89264	0.88923	0.91956	0.91165
Bus3	0.75932	0.74094	0.76727	0.75224
Bus4	0.73748	0.74086	0.81655	0.80345
Bus5	0.76214	0.76757	0.84161	0.82977
Bus6	0.81924	0.83625	0.94378	0.93282
Bus7	0.78969	0.80221	0.91208	0.89938
Bus8	0.93511	0.94304	1.0099	1.0024
Bus9	0.72905	0.74587	0.89255	0.87733
Bus10	0.72392	0.74231	0.89501	0.87959
Bus11	0.76108	0.77959	0.91591	0.90226
Bus12	0.77332	0.79402	0.92785	0.91496
Bus13	0.75599	0.77805	0.92092	0.90724
Bus14	0.68821	0.71354	0.88901	0.87218

After identifying the cases for which there is maximum deviation in the voltages, using the Cat Swarm Optimization technique, we find the optimal location and size of UPFC to

improvise the maximum loading limit of the system and also to bring the system voltages back to the pre disturbance values (or) near pre-disturbance values. We are incorporating three UPFC's based on the results obtained by observing the voltage magnitude profile at different buses. The reason for taking only three devices is purely based on voltage magnitude profiles of the system buses and the economic viability. The UPFC locations are based upon the contingent conditions observed as part the generator outage contingency analysis considered to be preview analysis. The voltages of buses 2 and 3 are observed to be low, even after erecting UPFC and during contingency for the reason due to the initial conditions considered as part of the system data.

Table 2 – Selected architecture of the neural network.

	Without any Load Model	With ZIP Load	With VD Load	With FD Load	With ER Load
Maximum Loading Parameter (λ_{max})	2.375	2.653	2.7571	3.1718	3.14

VD : Voltage Dependant
FD : Frequency Dependant
ER : Exponential Recovery

Table 3 – Voltage Magnitude Profiles for n-1 Generator Outage Contingencies.

Bus. No.	Generator2 contingency	Generator3 contingency	Generator6 contingency	Generator8 contingency
Bus1	1.0567	1.0573	1.0578	1.0577
Bus2	0.8654	0.90921	0.94851	0.9468
Bus3	0.83462	0.63846	0.88584	0.88123
Bus4	0.76674	0.74524	0.7753	0.7781
Bus5	0.78377	0.78206	0.78519	0.80179
Bus6	0.84667	0.84777	0.6188	0.80123
Bus7	0.80842	0.79897	0.75073	0.68728
Bus8	0.94893	0.94258	0.91456	0.68728
Bus9	0.74593	0.74036	0.64519	0.64628
Bus10	0.74119	0.73773	0.61473	0.64798
Bus11	0.78286	0.7821	0.60458	0.71204
Bus12	0.79818	0.80089	0.56428	0.74493
Bus13	0.77869	0.78153	0.55067	0.71966
Bus14	0.70172	0.70264	0.52881	0.61031

For installing the UPFC, its size in terms of VAR rating is determined using Cat Swarm Optimization technique. The optimum size of the UPFC's used here in terms of its converter ratings vary from one load type to another with 50% gain and a Time constant of 0.1. The UPFC is used in constant voltage mode. Maximum values of V_p, V_q and I_q are 1.15, 1.15 and 1.1 in P.U. and Minimum values of V_p, V_q and I_q are 0.85, 0.85 and 0.9 respectively.

For installing the UPFC, its size in terms of VAR rating is determined using Cat Swarm Optimization technique. The optimum size of the UPFC's used here in terms of its converter ratings vary from one load type to another with 50% gain and a Time constant of 0.1. The UPFC is used in constant voltage mode. Maximum values of V_p, V_q and I_q are 1.15, 1.15 and 1.1 in P.U. and Minimum values of V_p, V_q and I_q are 0.85, 0.85 and 0.9 respectively.

The Parameters that constitute the dimensions of the position of CAT in this case are :

No. of Iterations carried for CSO : 50

No. of Cats used : 03

No. of Cats in seeking mode : 02

No. of Cats in tracing mode : 01

Amongst the three UPFC's used, two UPFC's are taken in seeking mode and one is taken in tracing mode respectively. The location is decided based on contingency analysis given in table 3. 50 numbers of iterations are run for this technique, of which the global best solution is taken in to consideration. Table 4 shows the improvement in voltage profile and maximum loading parameter for ZIP load with generator6 contingency when three UPFC's are used in the bus locations 14-13, 5-4, and 14-9 with size 1kvar, 1kvar, and 0.15kvar respectively. Table 5 shows the improvement in voltage profile and maximum loading parameter for Voltage Dependant load with generator6 contingency when three UPFC's are used in the bus locations 14-13, 5-4, and 14-9 with size 0.7kvar, 1kvar, and 1kvar respectively. Table 6 shows the improvement in voltage magnitude profile and maximum loading parameter for Frequency Dependant load with generator6 contingency when three UPFC's are used in the bus locations 14-13, 5-4, and 14-9 with size 1kvar, 1kvar, and 1kvar respectively. Table 7 shows the improvement in voltage magnitude profile and maximum load-ability limit for Exponential Recovery load with generator6 contingency when three UPFC's are used in the bus locations 14-13, 5-4, and 14-9 with size 1kvar, 1kvar, and 0.15kvar respectively. Finally, it is observed near bus4, bus5, bus9, bus13 and bus 14 for which a deterioration of voltages happened for various load models under generator6 outage contingency. This was overcome by incorporating UPFC. The objective function for load modeling is achieved by improving the voltage magnitude profile to near 1 P.U. and maximum loading parameter also improved. The bar graphs in Fig. 4, Fig. 6, Fig. 8 and Fig. 10 and PV curves in Fig. 5, Fig. 7, Fig. 9 and Fig. 11 also depict the same.

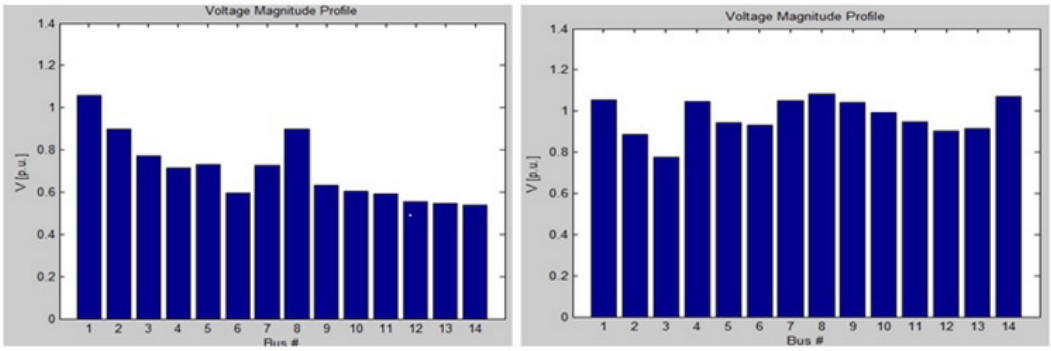

Fig. 4 – Voltage magnitude profile before and after placement of UPFC's (ZIP Load).

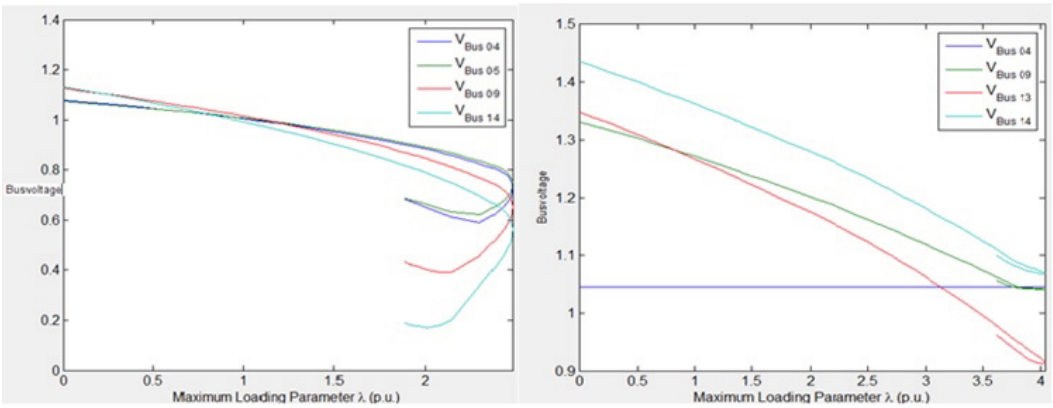

Fig. 5 – PV curves before and after placement of UPFC's (ZIP Load).

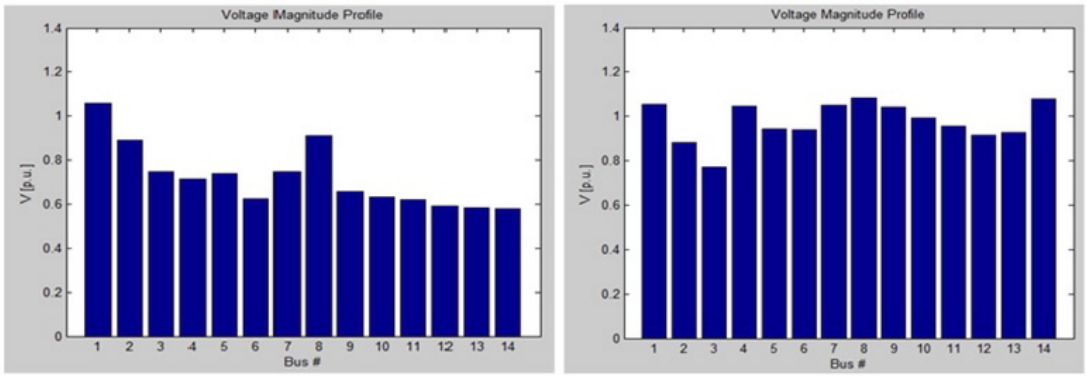

Fig. 6 – Voltage magnitude profile before and after placement of UPFC's (Voltage Dependant Load).

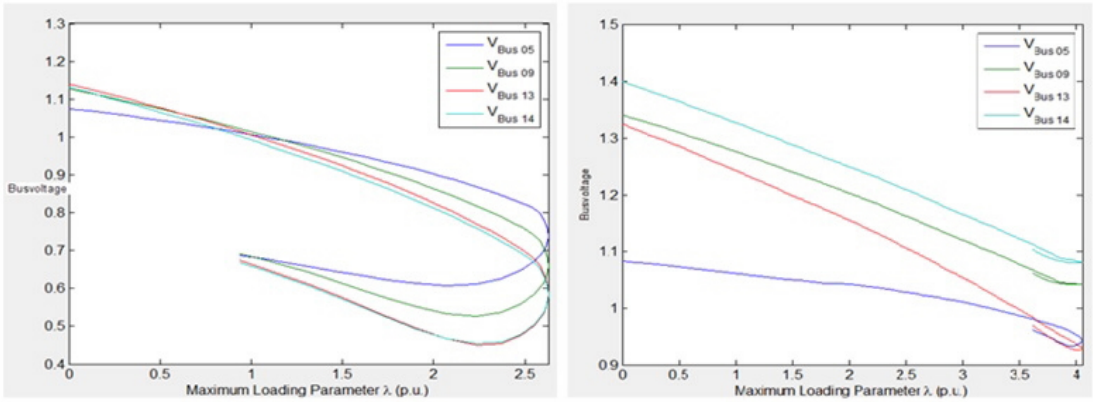

Fig. 7 – PV curves before and after placement of UPFC's (Voltage Dependant Load).

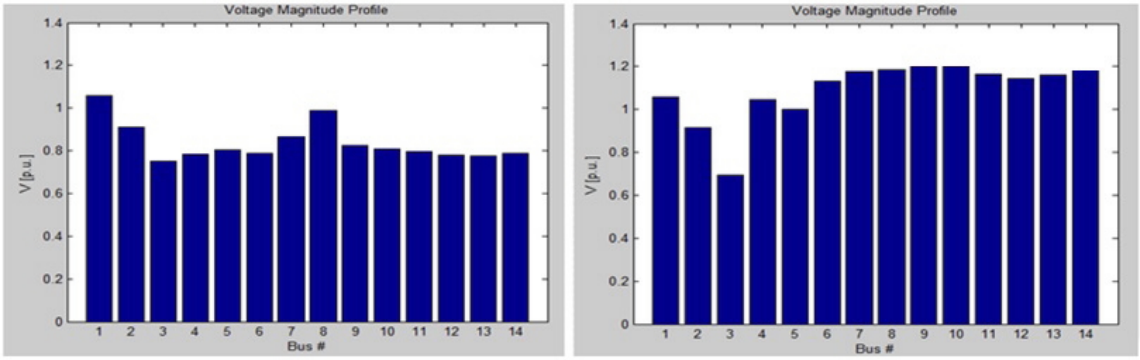

Fig. 8 – Voltage magnitude profile before and after placement of UPFC's (Frequency Dependant Load).

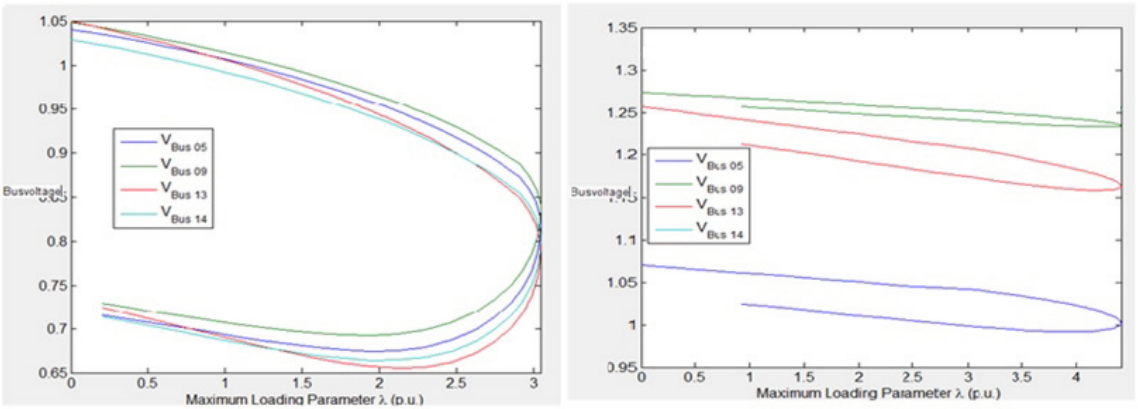

Fig. 9 – PV curves before and after placement of UPFC's (Frequency Dependant Load).

The reason for choosing three UPFC devices lies in the fact that the economy in installing the devices and operating them also plays a prominent role. In present day scenario, it costs approximately 80 USD per one KVAR to operate. This approximates to 5000 INR for operation in India. UPFC has both real and reactive power components but in this paper only reactive power is considered for the reason that the load centers have a direct impact on reactive power consumption. Various load models considered here show a deficit in reactive power for which reactive power compensation is provided. Though STATCOM and SVC devices are present, we are interested in showing a solution using advanced heuristic and FACTS technologies rather than resorting to primitive solutions.

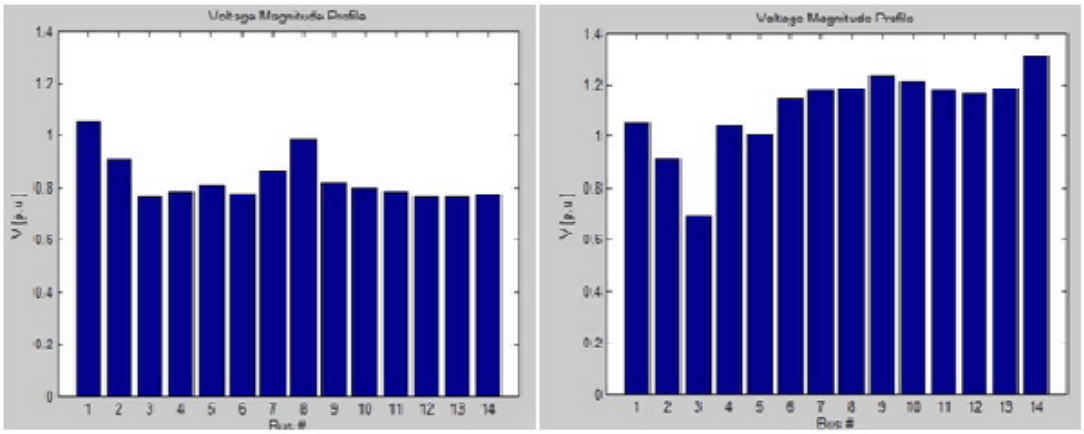

Fig. 10 – Voltage magnitude profile before and after placement of UPFC's (Exponential Recovery Load).

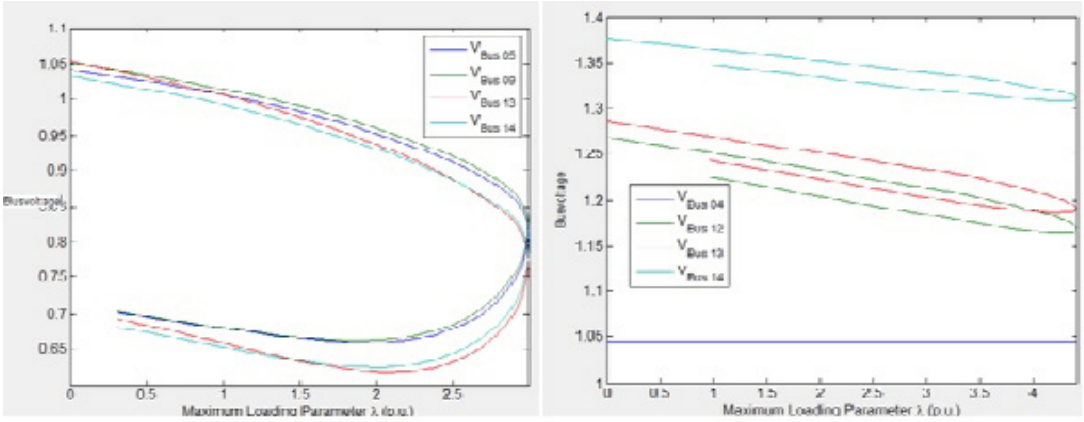

Fig. 11 – PV curves before and after placement of UPFC's (Exponential Recovery Load).

Table 4 – Voltage Magnitude Profile before and after generator6 outage contingency for ZIP load.

BUS. NO.	V(P.U) before Contingency with ZIP Load (Without UPFC's)	V(P.U) after Contingency with ZIP Load (Generator6)	V(P.U) after Contingency with ZIP Load (With 3 UPFC's)
01	1.0566	1.0566	1.0566
02	0.89264	0.89682	0.88534
03	0.75932	0.77122	0.77642
04	0.73748	0.71229	1.045
05	0.76214	0.7312	0.94191
06	0.81924	0.5936	0.93158
07	0.78969	0.72699	1.048
08	0.93511	0.89847	1.0809
09	0.72905	0.63318	1.041
10	0.72392	0.60518	0.99179
11	0.76108	0.58968	0.94877
12	0.77332	0.55395	0.90409
13	0.75599	0.54552	0.91522
14	0.68821	0.5402	1.069
MLP (λ_{max})	2.653	2.4808	4.0395

Table 5 – Voltage Magnitude Profile before and after generator6 outage contingency for Voltage Dependant Load.

BUS. NO.	V(P.U) before Contingency with VD Load (Without UPFC's)	V(P.U) after Contingency with VD Load (Generator6)	V(P.U) after Contingency with VD Load (With 3 UPFC's)
01	1.05660	1.0566	1.0566
02	0.88923	0.89083	0.88406
03	0.74094	0.74525	0.77031
04	0.74086	0.71576	1.045
05	0.76757	0.73732	0.94359
06	0.83625	0.62234	0.94094
07	0.80221	0.74553	1.0482
08	0.94304	0.91107	1.081
09	0.74587	0.65817	1.0419
10	0.74231	0.63285	0.9942
11	0.77959	0.61913	0.95433
12	0.79402	0.58976	0.9161
13	0.77805	0.58288	0.92837
14	0.71354	0.58004	1.0807
MLP (λ_{max})	2.7571	2.6285	4.0534

Table 6 – Voltage Magnitude Profile before and after generator6 outage contingency with Frequency Dependant Load.

BUS. NO.	V(P.U) before Contingency with FD Load (Without UPFC's)	V(P.U) after Contingency with FD Load (Generator6)	V(P.U) after Contingency with FD Load (With 3 UPFC's)
01	1.0572	1.0572	1.0572
02	0.91956	0.90944	0.91451
03	0.76727	0.74971	0.69206
04	0.81655	0.78305	1.045
05	0.84161	0.80494	1.0001
06	0.94378	0.78668	1.131
07	0.91208	0.86449	1.1782
08	1.0099	0.98705	1.1855
09	0.89255	0.82281	1.2339
10	0.89501	0.81029	1.2073
11	0.91591	0.79597	1.1663
12	0.92785	0.77815	1.1426
13	0.92092	0.77753	1.1614
14	0.88901	0.78815	1.0837
MLP (λ_{max})	3.1718	3.0441	4.4052

Table 7 – Voltage Magnitude Profile before and after generator6 outage contingency with Exponential Recovery Load.

BUS. NO.	V(P.U) before Contingency with ER Load (Without UPFC's)	V(P.U) after Contingency with ER Load (Generator6)	V(P.U) after Contingency with ER Load (With 3 UPFC's)
01	1.057	1.057	1.057
02	0.91165	0.91466	0.91794
03	0.75224	0.76788	0.69561
04	0.80345	0.78675	1.045
05	0.82977	0.80683	1.0046
06	0.93282	0.78063	1.1498
07	0.89938	0.86135	1.1813
08	1.0024	0.98513	1.1884
09	0.87733	0.81587	1.2379
10	0.87959	0.80206	1.2152
11	0.90226	0.7881	1.18
12	0.91496	0.76894	1.1663
13	0.90724	0.76751	1.1884
14	0.87218	0.77622	1.3099
MLP (λ_{max})	3.14	2.9936	4.422

5. Conclusion

The work presented here details a load model study for voltage stability using Cat Swarm Optimization. The case study considered was modeled using different static loads in generator outage contingency condition and analyzed for their performance in terms of voltage magnitude profile and maximum loading parameter. The different load models show an impact of instability in the system for which a solution is given using UPFC. A method is also presented to determine the optimal location and size of UPFC to enhance the stability. This method is based on Cat Swarm Optimization (CSO). This algorithm is in implementing compared to earlier AI techniques. It is capable of finding multiple optimal solutions, giving more flexibility to make the final decision about the location of the FACTS controller. On conclusion, we present application of an advanced technique to address stability issues arising in large power systems when connected and operated with different load models. The future scope of this work deals with the testing of above techniques for higher order IEEE case studies and practical networks.

REFERENCES

[1] Lakshman Pappula, Debalina Ghosh, "Linear Antenna Array Synthesis using Cat Swarm Optimization", International Journal of Electronics and Communication, Elsevier, Volume 68, Issue 6, June 2014, pages 540-549.

[2] Cheng Hong Gu, Qian Ai, Jiayi Wu, "A Study of Effect of Different Static Load Models and System Operating Constraints on Static Voltage Stability", Proceedings of the 5th WSEAS/IASME International Conference on Systems Theory and Scientific Computation, Malta, September 15-17, 2005 pp 44-49.

[3] Pei-Wei Tsai, Jeng Shyang Pan, Shyi-Ming Chen and Bin-Yih Liao, "Enhance Parallel Cat Swarm Optimization method based on the Taguchi Method", Expert Systems with Applications, Volume 39, Issue 7, pages 6309-6319, 2012.

[4] John J Paserba, "How FACTS Controllers Benefit AC Transmission Systems", Transmission and Distribution Conference and Exposition, 2010, IEEE PES, New Orleans, LA, USA.

[5] "Proposed Terms and Definitions for Flexible AC Transmission System (FACTS)", IEEE Transactions on Power Delivery, Volume 12, 1997.

[6] F Milano, "Power System Analysis Toolbox", Version 1.3.4, Software and Documentation, July 14, 2005.

[7] "Power System Analysis Toolbox Documentation for PSAT version 2.0.0 β", March 8, 2007.

[8] A Kazemi, V Vahidinasab, A Mosallanejad, "Study of STATCOM and UPFC Controllers for Voltage Stability Evaluated by Saddle-Node Bifurcation Analysis", First International Power and Energy Conference, November 28-29, 2006, Putrajaya, Malaysia.

[9] Musunuri S, Dehnavi G, "Comparison of STATCOM, SVC, TCSC & SSSC Performance in Steady State Voltage Stability Improvement", North American Power Symposium (NAPS), 26-28 Sept. 2010, pages 1– 7.

[10] Kalaiselvan G, Lavanya A, Natrajan V, "Enhancing the Performance of Watermarking Based on Cat Swarm Optimization Method", IEEE International Conference on Recent Trends in Information Technology, Anna University, Chennai, June 3-5, 2011.

[11] Jong Ching Hwang, Jung Chin Chen, J S Pan, Yi Chao Huang, "CSO and PSO to Solve Optimal Contract Capacity for High Tension Customers", IEEE, PEDS 2009.
[12] Budi Santosa, Mirsa Kencana Ningrum, "Cat Swarm Optimization for Clustering", International Conference on Soft Computing and Pattern Recognition, 2009.
[13] Wen Zing, Adeline Chan, "Power System Load Modelling", The School of Information Technology and Electrical Engineering, University of Queensland, October 2003.
[14] C W Taylor, "Power System Voltage Stability", New York, McGraw-Hill, 1994.
[15] Prabha Kundur, Neal J Balu, Mark G Lauby, "Power Systems Dynamics and Stability", McGraw-Hill, 01-Jan-1994.
[16] Hingorani N G, Gyugyi L, "Understanding FACTS : Concepts and Technology of Flexible AC Transmission Systems", IEEE Press, New York, 2000.

Authors

Dr G Naveen Kumar obtained his B.Tech, M.Tech and PhD from Jawaharlal Nehru Technological University, Hyderabad. He is currently working as Assistant Professor in Electrical and Electronics Engineering department at VNR Vignana Jyothi Institute of Engineering and Technology, Hyderabad, India. His research interests include embedded system applications to power systems problems.

p-ISSN : 2335-1357 e-ISSN : 2437-1122

Mediterranean Journal of Modeling and Simulation

Med. J. Model. Simul. 05 (2016) 017-028

The Impact of TCSC on IDMT Relays in SLG Fault in Distribution Networks

Lazhar Bougouffa [a] *, Abdelaziz Chaghi [a]

[a] LSP-IE Laboratory Research Laboratory, Faculty of Technology, Department of Electrical of Engineering, University of Batna - Algeria

ARTICLE INFO

Article history :
Received January 2016
Accepted March 2016

Keywords :
Power system ;
IDMT ;
DOCRTCSC ;
SLG. Fault resistance (RF).

ABSTRACT

IDMT Directional Over-Current Relays protection is one of the basic protective relaying for distribution systems, for fault detection and clearing as soon as possible. Its function would generally be changed in presence of FACTS devices. In this paper a study to investigate the direct effect of varying reactance of the TCSC on single-line-to-ground (SLG) fault in compensated distribution systems. This paper, therefore presents the calculation of fault component, and directional over-current relay operating time characteristics for phase-to-earth fault involving the TCSC. The case study is compared between compensated and uncompensated system. The coordination of the relays is a nonlinear programming problem and it is solved by using MATLAB software.

1. Introduction

The equipments of electric power systems represent some of the oldest industrial machinery still in general use today. Another dimension of automation in the case of transmission systems is the direct modification of the grid's properties with the aid of solid-state technology essentially ; various types of transistors scaled up and combined to handle large power applications in a new category of equipments called flexible A.C. transmission systems (FACTS). Transmission lines generally have physically fixed parameters such length and impedance that become firm constraints in modeling and analysis. Other components such as transformers and capacitors may have variable states or settings, but conventionally these settings are discrete and require mechanical switching. FACTS technology offers ways to modify the electrical characteristics of transmission components much more rapidly, even in real time, so as to increase operating efficiency and relieve constraints without the need for adding major equipments. FACTS devices include various types of reactive compensation, phase shifting, and power flow control [1]. The idea is to

*Email : blazhar2010@gmail.com

effectively change the impedance of a given transmission link as seen by the system on an instantaneous basis by means of an appropriately designed solid-state electronic circuit.

However the fault location in distribution networks shows known problems because of the network branching, laterals and dynamical change of loads along the network sections. The problem is made more difficult when the network neutral is isolated or compensated. In such networks a fault current during the phase-to-ground fault considerably depends on the network capacitance and has a resonant character [1]. The fault-loop impedance is relatively high, which results in low fault current. The fundamental component fault current and voltage phasors do not contain information on distance to fault [2]. Over-current protection is one of the basic protective relaying principles for distribution systems. An over-current relay must be capable of protecting the zone under its primary protection and only if the primary protection system does not clear the fault, the back-up protection should initiate tripping. Mal-operation of the backup relays should be avoided to reduce power outages. The relay's mal-operation includes fail-to-trip or mal-trip. Fail-to-trip event occurs when the relay fails to trip in the presence of faults and mal-trip event occurs when the relay trips even though it is in healthy condition. A mal-trip event results in more severe damage to the system compared to fail-to-trip event [3].

The authors in [4] study the effects of GCSC on fault current and DOCRs operation time in the presence of phase to earth fault with fault resistance. Our paper, therefore presents the calculation of fault component, and directional over-current relay operating time for single-line-to-ground fault involving a TCSC compensator. The TCSC will be always present in the fault loop and will influence the relay setting characteristic. The effects of the earth fault resistance and TCSC control parameters on the settings of both primary relay and backup relay is investigated in this paper.

2. TCSC structure and operation

The basic Thyristor Controlled Series Capacitor scheme, proposed in 1986 by Vithayathil with others as a method of "rapid adjustment of network impedance," is shown in Fig.1 [5]-[6]. It consists of the series compensating capacitor shunted by a Thyristor Controlled Reactor.

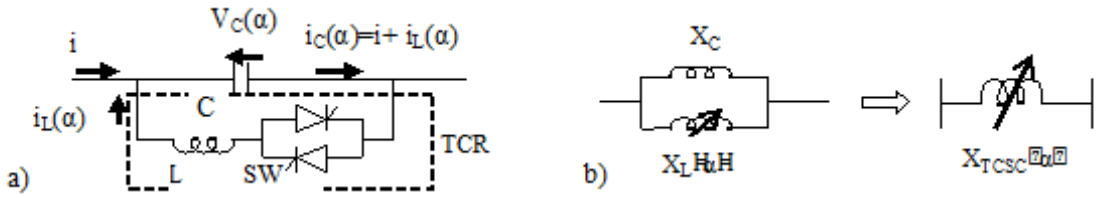

Fig. 1 – Principal of TCSC (a) Basic TCSC scheme and (b) Apparent TCSC reactance.

In a practical TCSC implementation, several such basic compensators may be connected in series to obtain the desired voltage rating and operating characteristics. However, the basic idea behind the TCSC scheme is to provide a continuously variable capacitor by means of partially canceling the effective compensating capacitance by the TCR [4]. Since,

the TCR at the fundamental system frequency is a continuously variable reactive impedance, controllable by delay angle α, the steady-state impedance of the TCSC is that of a parallel LC circuit, consisting of a fixed capacitive impedance, X_c, and a variable inductive impedance, $X_L(\alpha)$, that is,

$$X_{TCSC}(\alpha) = \frac{X_L(\alpha) \times X_C}{X_L(\alpha) + X_C} \tag{1}$$

Where : XL = ωL

The TCSC thus presents a tunable parallel LC circuit to the line current that is substantially a constant alternating current source. As the impedance of the controlled reactor, X_L (α). Is varied from its maximum (infinity) toward its minimum (ωL), the TCSC increases its minimum capacitive impedance, X^{min}_{TCSC} =$X_c = 1/\omega C$, (and thereby the degree of series capacitive compensation) until parallel resonance at $X_c = X_L$ (α) is established and X^{max}_{TCSC} theoretically becomes infinite [6].

TCSCs vary the electrical length of the compensated distribution system with little delay. This characteristic enables the TCSC to be used to provide fast active power flow regulation.

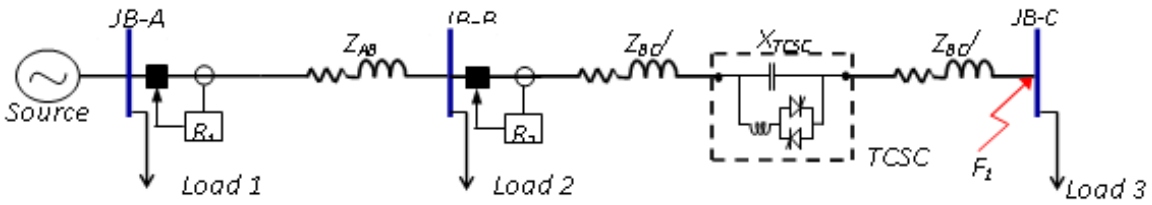

Fig. 2 – Diagram of distribution path with TCSC.

The rated value of TCSC is a function of the reactance where the TCSC is installed and expressed as :

$$X_{line} = X_{BC} + X_{TCSC} \tag{2}$$

Where

$$X_{TCSC} = K_{TCSC} \times X_{line} \tag{3}$$

X_{line} is the overall line reactance between bus-B and C with TCSC installation. XTCSC is the reactance of TCSC and KTCSC is the coefficient which represents the compensation level of TCSC ($-0.7 \leqslant K_{TCSC} \leqslant 0.2$). The working range of reactance of TCSC is fixed between -0.7 (capacitive) X_{line} and 0.2 (inductive) X_{line} [7-9].

3. Directional over-current relay coordination

Inverse Definite Minimum Time (IDMT) directional over-current relay is inverse in the initial part, which tends to definite minimum operating time as the current becomes very high. The reason for the operating time becoming definite minimum, at high values of current, is that in the electromechanical relays the flux saturates at high values of current. Ideally, we may demand that the operating time inverse in nature throughout the operating range [10]. The mathematical relation between the current and the operating time of IDMT characteristic can be written as :

$$T = TDS \times \frac{a}{M^b - 1} \tag{4}$$

Where :
M is the multiple of pickup current
TDS is the time dial setting of the relay.
Where, a and b are constants depending on the type of selected characteristics [3] : Standard Inverse (SI), Very Inverse (VI) or Extremely Inverse (EI) and Long time inverse are indicated in Tables 1.

Table 1 – Parameters for different inverse characteristics.

Inverse characteristics	a	b
Standard inverse	0.2	0.14
Very inverse	1	13.5
Extremely inverse	2	80
Long time inverse	1	120

3.1. Backup-primary constraint

In order to coordinate two over-current relays, one as primary relay (i) and the other as backup relay (j), the difference between the operation time of backup relay and main relay should be more than Coordination Time Interval (CTI). So the constraints for coordination of over-current relays (i) and (j) will be in the form of inequality (5), if R_i is the primary relay for fault at k, and R_j is backup relay for the same fault, the Coordination constraint can be stated as [11]-[12] ;

$$T_j^K - T_i^K \geq CTI \tag{5}$$

T_j^K and T_i^K time interval for coordination of primary and backup relay and it can take a value between 0.2 and 0.5 seconds. In this paper we selected 0.3 s of CTI [12]-[13].

The essence of the directional over-current relay coordination study is the calculation of its TDS and IP. It worth mentioning that DOCR allow for continuous time dial setting, but rather discrete pickup current setting [14]. Formulating the above constraints gives :

$$TDS_i^{\min} \leq TDS_i \leq TDS_i^{\max} \tag{6}$$

$$I_{pi}{}^{\min} \leq I_{pi} \leq I_{pi}{}^{\max} \tag{7}$$

4. Single line to ground fault current calculation with TCSC

Figure 3 shows the connection of the sequence networks for a single-line-to-ground fault (A–G fault) in presence of TCSC installed at midpoint of branch BC. The sequence networks are connected in series and additionally the triple fault resistance (3.RF) is included.

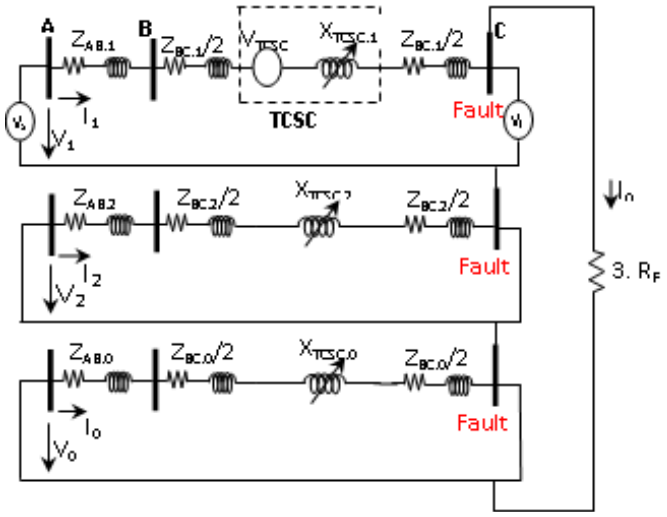

Fig. 3 – Equivalent circuit diagram of the single-line-to-ground fault (A-G fault) involving fault resistance R_F in presence of TCSC installed at midpoint.

The total impedance of system with TCSC ($Z_{BC-Total}$) is :

$$Z_{BC-Total} = R_{BC} + j\left[X_{BC} - X_{TCSC}\left(\alpha\right)\right] \tag{8}$$

At fault occurrence at bus-bar C the basic equations for this type of fault [4] are :
The direct component of currents in presence TCSC on midline is :

$$I_1 = \frac{V_s + V_{TCSC}}{Z_{AB-T} + \left(\frac{Z_{BC-T}}{2}\right) + X_{TCSC-T} + \left(\frac{Z_{BC-T}}{2}\right) + 3R_f} \tag{9}$$

And :

$$I_1 = I_2 = I_0 \tag{10}$$

Where the indices T is the sum of Symmetrical components (direct, inverse and zero components).

The current at phase (A) current in presence TCSC on midline is given by :

$$I_a = \frac{3 \times (V_s + V_{TCSC})}{Z_{AB-T} + \left(\frac{Z_{BC-T}}{2}\right) + X_{TCSC-T} + \left(\frac{Z_{BC-T}}{2}\right) + 3R_f} \tag{11}$$

The current at phase (B) and phase (C) currents are :

$$I_b = I_c = 0 \tag{12}$$

The direct, inverse and zero components of voltage in presence of TCSC on midline is :

$$\begin{aligned} V_1 &= V_s + V_{TCSC} - \left[Z_{AB-1} + \left(\frac{Z_{BC-1}}{2}\right) + X_{TCSC-1} + \left(\frac{Z_{BC-1}}{2}\right)\right].I_1 \\ &= \frac{(V_s+V_{TCSC}).\left[Z_{AB}{}'+Z_{BC}{}'+X_{TCSC}{}'+3R_f\right]}{Z_{AB-T}+\left(\frac{Z_{BC-T}}{2}\right)+X_{TCSC-T}+\left(\frac{Z_{BC-T}}{2}\right)+3R_f} \end{aligned} \tag{13}$$

$$\begin{aligned} V_2 &= -\left[Z_{AB-2} + \left(\frac{Z_{BC-2}}{2}\right) + X_{TCSC-2} + \left(\frac{Z_{BC-2}}{2}\right)\right].I_2 \\ &= -\frac{(V_s+V_{TCSC}).[Z_{AB-2}+Z_{BC-2}+X_{TCSC-2}]}{Z_{AB-T}+\left(\frac{Z_{BC-T}}{2}\right)+X_{TCSC-T}+\left(\frac{Z_{BC-T}}{2}\right)+3R_f} \end{aligned} \tag{14}$$

$$\begin{aligned} V_0 &= -\left[Z_{AB-0} + \left(\frac{Z_{BC-0}}{2}\right) + X_{TCSC-0} + \left(\frac{Z_{BC-0}}{2}\right)\right].I_0 - R_f.I_0 \\ &= -\frac{(V_s+V_{TCSC}).\left[Z_{AB-0}+Z_{BC-0}+X_{TCSC-0}+R_f\right]}{Z_{AB-T}+\left(\frac{Z_{BC-T}}{2}\right)+X_{TCSC-T}+\left(\frac{Z_{BC-T}}{2}\right)+3R_f} \end{aligned} \tag{15}$$

The voltages in presence TCSC on midline is given by :
Single line-to-ground fault voltage with TCSC is given by :

$$V_{a-g} = R_f \times I_a \tag{16}$$

$$V_{A-G} = \frac{3.R_f.\,(V_s + V_{TCSC})}{Z_{AB-T} + \left(\frac{Z_{BC-T}}{2}\right) + X_{TCSC-T} + \left(\frac{Z_{BC-T}}{2}\right) + 3R_f} \tag{17}$$

$$V_B = \frac{(V_s + V_{TCSC})\,.\,[(a^2 - a)Z_2{}' + (a^2 - 1)Z_0{}' + T_a.R_f]}{Z_{AB-T} + \left(\frac{Z_{BC-T}}{2}\right) + X_{TCSC-T} + \left(\frac{Z_{BC-T}}{2}\right) + 3R_f} \tag{18}$$

$$V_C = \frac{(V_s + V_{TCSC})\,.\,[(a - a^2)Z_2{}' + (a - 1)Z_0{}' + T_b.R_f]}{Z_{AB-T} + \left(\frac{Z_{BC-T}}{2}\right) + X_{TCSC-T} + \left(\frac{Z_{BC-T}}{2}\right) + 3R_f} \tag{19}$$

Where :

$$X_{TCSC}{}' = X_{TCSC-2} + X_{TCSC-0} - 2.X_{TCSC-1} \tag{20}$$

$$Z_{AB}{}' = Z_{AB-2} + Z_{AB-0} - 2.Z_{AB-1} \tag{21}$$

$$Z_{BC}{}' = Z_{BC-2} + Z_{BC-0} - 2.Z_{BC-1} \tag{22}$$

$$Z_2{}' = Z_{AB-2} + Z_{BC-2} + X_{TCSC-2} \tag{23}$$

$$Z_0{}' = Z_{AB-0} + Z_{BC-0} + X_{TCSC-0} \tag{24}$$

$$T_a = (3.a^2 - 1) \tag{25}$$

$$T_b = (3.a - 1) \tag{26}$$

5. Case study and results

The case study based on Fig. 2 shows a part of 11-kV distribution network, where : the positives impedances of branches from A to B : $Z_{AB} = 0.922 + 0.470j$, and from B to C : $Z_{BC} = 0.4930 + 0.2511j$. Positive and negative sequence impedances are assumed equal and zero sequence impedance are assumed three of positive sequence impedance. With the given parameters of a TCSC, the values of capacitor and inductor are 213.5 μF and 9.57mH respectively.

Two branches protected by R1 and R2, which are directional over-current relays. Each protective relays is assigned a primary function to clear faults in a specific zone and a backup function to clear faults in another zones. The over-currant relay characteristics can be seen by using the IEC standard inverse curve.

The single-phase fault applied in this study is phase A to earth at bus-3 with a variable fault resistance. With a variable fault resistance and the TCSC operation for fault durations. The case study presented simulations results of current and voltage symmetrical components and phase's values are presented in Figures 5, 6, 7 and 8 respectively.

Fig.5 represent the variation of the symmetrical components of currants I_1, I_2 and I_0 respectively and Fig.6 represent the variation of Three phases currents on distribution line as a function RF varied from 0 to 100 Ω on inductive and capacitive modes.

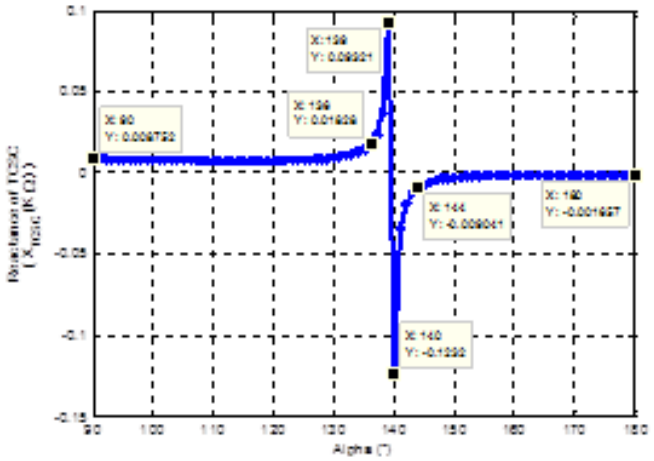

Fig. 4 – Characteristic Curve of TCSC study $X_{TCSC}(\alpha)$.

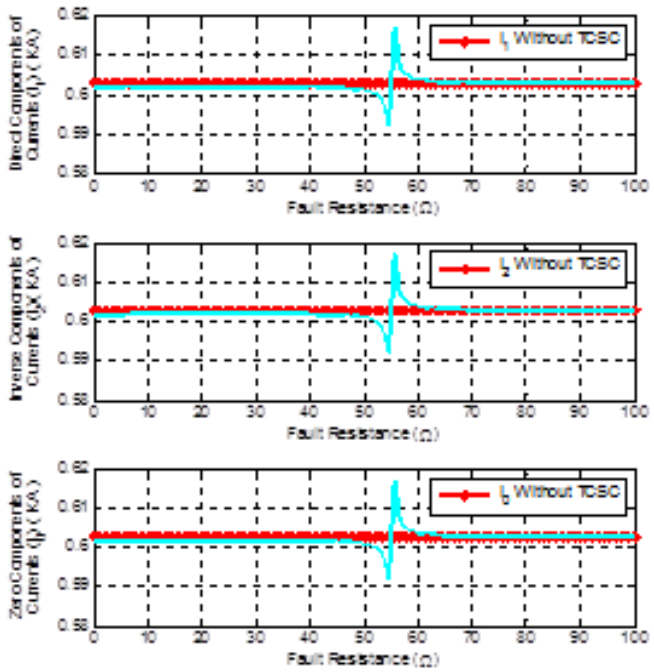

Fig. 5 – Symmetrical components of current.

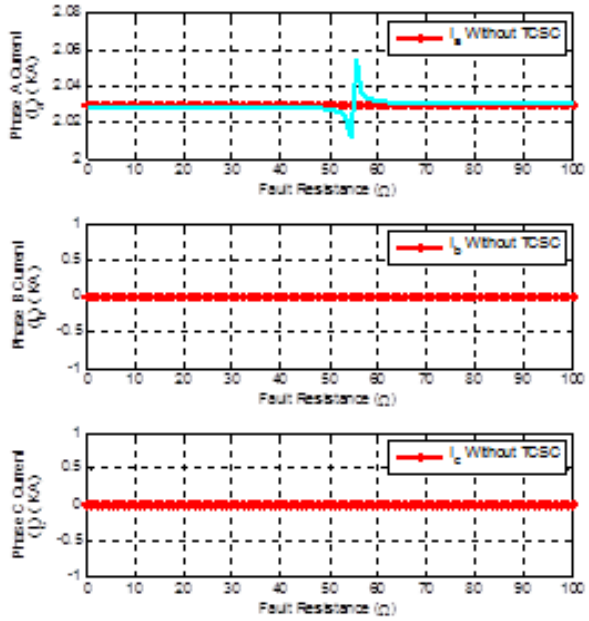

Fig. 6 – Three phases currents on distribution line.

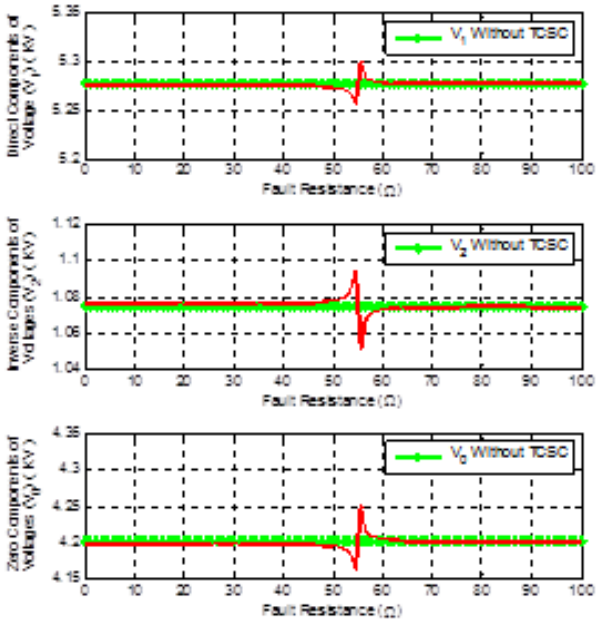

Fig. 7 – Symmetrical components of voltages.

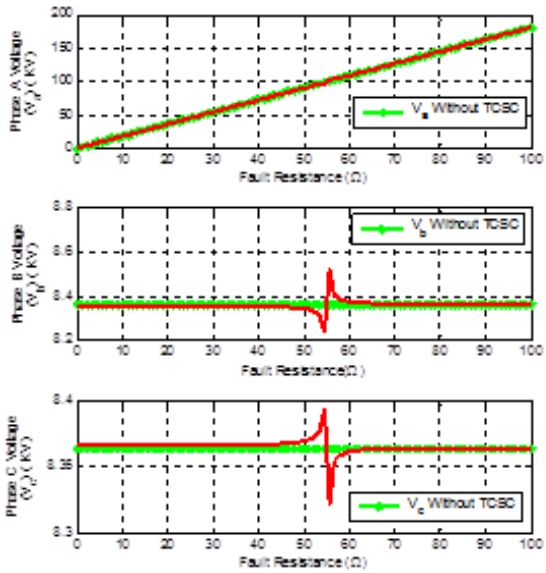

Fig. 8 – Three phases voltages on distribution line.

It is observed that the fault phase A to ground with resistance of default is large compared to those of without resistance. It can be seen as well that there is an effect of the inductive mode and capacitive mode on the voltage in phase B and C.

In fig. 9 PRC, BRC and O.T are Primary Relay Characteristic, Backup Relay Characteristic and Operating Time respectively.

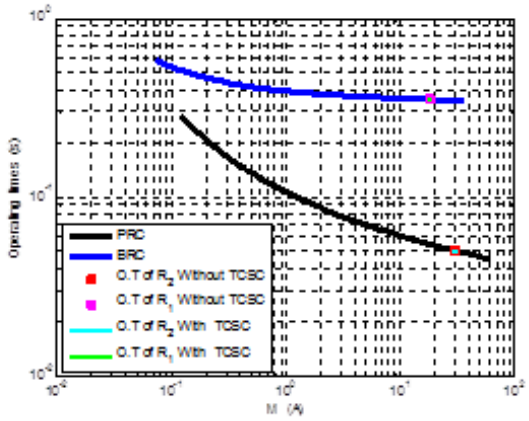

Fig. 9 – Operating times characteristics of primary and backup relays for Earth fault with and without TCSC.

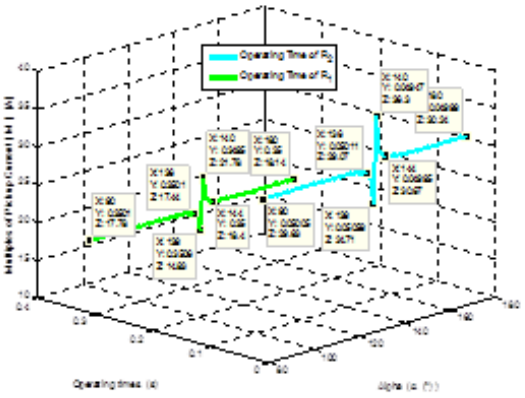

Fig. 10 – Zoom of Impact of TCSC modes on operating times of R2 and R1 for the fault F1.

It clears in Fig. 10 the effect of the varying reactance of the TCSC with firing angle alpha on operating time of the relays. Where for a fixed $I_P = 1$, the value M is variable car the value of fault currant is variable on function of reactance injected by the TCSC.

6. Conclusion

The effects of TCSC compensator on the variation of three phase's currents on distribution line as a function of an earth fault R_F varied from 0 to 100 Ω in inductive and capacitive mode are presented. The impact of earth fault with the presence of a TCSC on the operating time for a primary relay is investigated. The effects of varying mode of TCSC on multiple of pickup current and operating times are clear in 3-D. The CTI is taken as 0.3s. The coordination of the relays is a nonlinear programming problem and it is solved by using MATLAB software.

REFERENCES

[1] Alexandra von Meier, Electric power systems, ISBN-13 : 978-0-471-17859-0, by John Wiley & Sons. 2006.

[2] M. M. Saha. J. Izykowski and E. Rosolowski, Fault Location on Power Networks, Power Systems. Published by Springer, October 2009.

[3] Yin L. G. Agileswari K. R. Farrukh H. N. and Aidil A. Z. A., DSP based over-current relay using fuzzy bang–bang controller, Microelectronics Reliability, 51, 2011, pp 2366–2373.

[4] M. Zellagui, R. Benabid, A.z Chaghi, M. Boudour, Impact of GCSC on IDMT Directional Over-current Relay in the Presence of Phase to Earth Fault, Serbian Journal of Electrical Engineering, 2014, pp1-18.

[5] R. M. Mathur and R. K. Varma, Thyristor-Based FACTS Controllers for Electrical Transmission system, IEEE Press, A JOHN WILEY & SONS, INC. Publication, 2002.

[6] G. H. Narain and G. Laszlo, "Understanding FACTS –Concepts and Technology of Flexible AC Transmission Systems", IEEE Press, 2000.

[7] S. S. Reddy, M. S. Kumari and M. Sydulu, Congestion Management in Deregulated Power System by Optimal Choice and Allocation of FACTS Controllers Using Multi-Objective Genetic Algorithm, Journal of Electrical Engineering & Technology Vol. 4, No. 4, 2009, pp.467-475.

[8] P. K. Tiwari, Y. R. Sood, An Efficient Approach for Optimal Placement of TCSC in Double Auction Power Market, International Journal of Electronics and Electrical Engineering (IJEEE), 2012, pp321-326.

[9] N. K. Easwaramoorthy and R. Dhanasekaran, Solution of Optimal Power Flow Problem Incorporating Various FACTS Devices, International Journal of Computer Applications Volume 55– No.4, October 2012, pp 38-44.

[10] Y.G. Paithankar and S.R. Bhide, Fundamentals of Power System Protection, Published by Prentice-Hall of lndia, New Delhi. ISBN-81-203-2194-4. 2003.

[11] D.Vijayakumar and R.K. Nema, Superiority of PSO Relay Coordination Algorithm over Non-Linear Programming : A Comparison, Review and Verification". IEEE 2008.

[12] B.K. Panigrahi, M. Singh and A.R. Abhyankar. "Optimal coordination of directional over-current relays using Teaching Learning-Based Optimization (TLBO) algorithm, Electrical Power and Energy Systems 50, 2013, pp 33–41.

[13] E. Mazhar, K. Robert, A novel method for optimal Coordination of directional over-current relays considering their available discrete settings and several operation characteristics, Electric Power Systems Research 81, 2011, pp 1475–1481.

[14] H. H. Zeineldin, E. F. El-Saadany and M. M. A. Salama, Optimal coordination of over current relays using a modified particle swarm optimization, Electric Power Systems Research 76, 2006, pp 988–995.

p-ISSN : 2335-1357 e-ISSN : 2437-1122

Mediterranean Journal of Modeling and Simulation

Med. J. Model. Simul. 05 (2016) 029-045

Performance evaluation of a wiener model predictive control for a coagulation chemical dosing unit in water treatment plants

O. Bello [a] *, Y. Hamam [b] , K. Djouani [c]

[a] Electrical Engineering Department, French South African Institute of Technology, Tshwane University of Technology, Private Bag X680, Pretoria, 0001, South Africa.
[b] French South African Institute of Technology, Tshwane University of Technology, Private Bag X680, Pretoria, 0001, South Africa.
[c] Electrical Engineering Department, University Paris Est-Creteil (UPEC), France.

ARTICLE INFO

Article history :
Received January 2016
Accepted March 2016

Keywords :
Water treatment ;
Coagulation ;
Wiener model ;
Model predictive control.

ABSTRACT

Coagulation process control is an essential operation in water treatment plants. It is a challenging control problem due to the nonlinear and physicochemical nature of the coagulation process. The paper presents the application of the Wiener model predictive control (WMPC) algorithm to a coagulation chemical dosing unit for water treatment plants in order to keep the surface charge and pH level of the dosed water at the reference trajectory set by the operator of the plant. Wiener models with different nonlinear estimators are compared and evaluated. A Wiener model with a wavelet network estimator presented the highest goodness of fit (98%), and was thus selected as the best prediction model. Simulation results show that the proposed control strategy has good set-point tracking, as well as noise and disturbance rejection performances.

1. Introduction

The coagulation process control is a challenging problem in the water and wastewater, paper and pulp, beverage and brewery industries where the need for clean water is imperative to achieve the organisation goals and objectives. This could be attributed to the complex and nonlinear behaviour of the process [1, 11]. Several approaches have been proposed in the literature for the control of the process in the water treatment plants in particular. Traditionally, visual inspection and reference table are methods used by plant operators to evaluate the quality of the finished water. The operators observe the water and make adjustment to increase, maintain or decrease the coagulant dosages based on

*engroobello@gmail.com

their personal judgment and experience. This approach does not support production of adequate and cost effective water treatment operation. Moreover, jar tests are basically routine laboratory procedures to establish the optimum dosage of coagulation chemicals for water treatment. A typical jar test apparatus consists of a six variable-speed paddle gang stirrers with impellers, 1.5 litres square glass beakers or jars and sample tap or draw-off siphoning tube. The jar tests could be suitably used to select primary and secondary coagulants, perform mixing energy and time studies, estimate the settling velocities for sedimentation, basin sizing and evaluate sludge recycling effect. However, jar tests are time-consuming and labour intensive. It does not have the ability to be incorporated into an online monitoring and automatic control scheme for coagulation process [9].

Another common approach is to develop prediction process models for coagulation chemical dosages using data collected from water treatment plants. The input variables of these models are obtained from the operational and physical water quality parameters of the raw water flowing into the plant. These parameters are measured by means of appropriate sensors before the water enters the rapid mixing tank or dosing point. These models are developed using statistical or regression analysis techniques [7]. Alternatively, intelligent techniques such as artificial neural networks, adaptive neuro-fuzzy inference scheme, fuzzy logic and genetic programming techniques are suitably used to model the nonlinear relationship between the input and output variables of the prediction models [2, 11, 12, 15–18]. Previous studies have shown that these intelligent techniques exhibit lesser prediction errors when compared to the regression based model [7]. With the development of these empirical models, feedforward controllers are implemented to control the flowrates of the dosing pumps with satisfactory results [3]. Automatic control actions of the coagulation chemical dosage system could also be provided using the feedback controllers. In this approach, streaming current detector and pH meter are required to achieve feedback of the measured variables to the control system. The streaming current detector provides a direct measurement of the average colloidal surface charge while the pH meter measures the pH or degree of hydrogen ions concentration in the raw water. For effective implementation of a feedback control scheme, the average colloidal surface charge and pH of the water after coagulation must be controlled to follow the reference trajectory set by the plant operators and have robust performance when operational disturbances are acting on the process [1], [13] and [7].

Model predictive control (MPC) is a widely used control algorithm in the process industries. It involves the use of a dynamic model to predict and optimise process performances. MPC has capability to handle system constraints effectively and could be used with multiple-input, multiple output systems where the traditional control scheme may prove inadequate. Most processes are nonlinear in nature, whereas most MPC software available are based on linear dynamic model. Thus, the MPC may not work effective with highly nonlinear processes. One of the identified approaches to approximate any nonlinear process with high precision is to use Wiener model. Wiener model has a structure that consists of the cascade connection of a linear invariant (LTI) system followed by a static or memoryless nonlinearity. The application of the Wiener model to nonlinear processes have been discussed and reported in [8, 14]. The most commonly used nonlinearity blocks will be applied in this study to identify a Wiener model from the input-output data generated from a nonlinear first principles simulation model of the coagulation process in a rapid

mixing tank reactor. The simulation model is developed based on the operational data collected from the Rietvlei water treatment plant, South Africa. The identification results of the nonlinearity blocks are compared to determine the best estimator among them. The best identified Wiener model is applied in the MPC algorithm. The performances of the Wiener model predictive control scheme are examined in terms of its ability to track changes in reference trajectory and reject disturbances after a simulation period of 48 hours.

2. Materials and methods

2.1. Description of the Rietvlei water treatment plant

The Rietvlei water treatment plant was built between 1932 and 1934, near Irene, City of Tshwane, South Africa. The production capacity of the plant is approximately 40 million litres per day. Fig. 1 illustrates the process train of the Rietvlei water treatment plant. A pumping station and transport system is available to lift water from the dam and convey it to the treatment plant. Raw water then flows through the intake pipe into the coagulation chemical dosing unit. The chemical dosing unit consists of a concrete mixing tank with inlet and outlet channels. Four metering pumps are used for dosing the chemicals into the influent raw water of which two dosing pumps are active while the other two are on a standby or redundant position. One of the dosing pumps feeds a polyelectrolyte solution while the other feeds a ferric chloride solution into the concrete mixing tank. The polyelectrolyte solution known as sudfloc 3835, is a blend of epichlorohydrin/dimethylamine (polyamine) and aluminium chlorohydrate. The adoption of organic polyelectrolytes as part of the water treatment process in South African waterworks is widely established due to their higher efficiency and lower cost when compared to the traditional or inorganic coagulants. The pumps are controlled by programmable logic controllers (PLC) that are connected to the supervisory control and data acquisition (SCADA) system of the plant. The dosage quantities of coagulation chemicals depend on the influent flowrate of the raw water flowing into the water treatment plant. Calcium hydroxide (hydrated lime) in slurry form is also added to the mixing tank using a diaphragm pump to stabilise the water and adjust the pH value to a set point value between 8.1 and 8.3.

The chemically dosed water flows out slowly and evenly from the rapid mixing tank into a series of baffled or flocculation channels to grow the flocs. The water from the baffled channels then flow into the Dissolved Air Floatation/Filtration (DAFF) unit. The filtered water from the DAFF then flows into the Granular Activated Carbon (GAC) filtration unit to eliminate any foul odour, taste and colour caused by the natural organic matter. Thereafter, the water from the GAC flows into the chlorination chamber. Here, chlorine gas is added to the water to disinfect the clean water before it is pumped to the storage reservoirs and distributed to end users [4, 5].

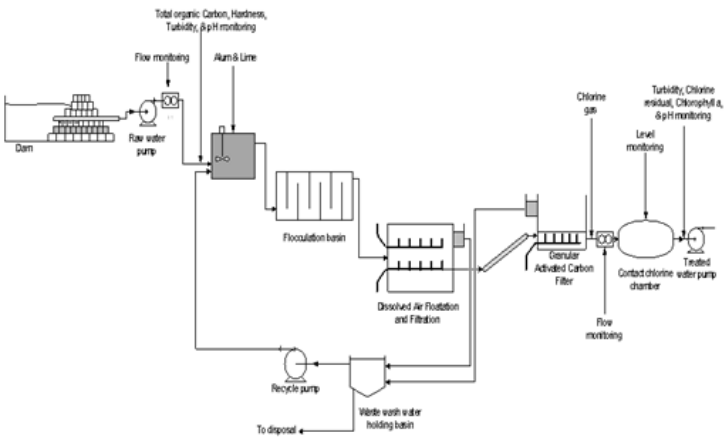

Fig. 1 – Process flow diagram of the Rietvlei water treatment plant, City of Tshwane.

2.2. Theoretical Modelling

The general chemical reactions in the mixing tank reactor in Fig. 2 are written as [5] :

$$\begin{aligned} &2\left(C_5H_{12}ONCl\right)_n + 2Al_2Cl\left(OH\right)_5 + 2Ca\left(HCO_3\right)_2 \rightarrow \\ &2\left(C_5H_{12}ON^+\right)_n + 4Al\left(OH\right)_3 + 2OH^- + 2CaCl_2 + 4CO_2 \end{aligned} \tag{1}$$

$$2FeCl_3 + 3Ca(HCO_3)_2 \rightarrow 2Fe(OH)_3 + 3CaCl_2 + 6CO_2 \tag{2}$$

$$Ca(HCO_3)_2 + Ca(OH)_2 \rightarrow 2CaCO_3 + 2H_2O \tag{3}$$

Chemical reactions in (1), (2) and (3) take place simultaneously. Therefore, the overall chemical equation becomes :

$$\begin{aligned} &2(C_5H_{12}ONCl)_n + 2Al_2Cl(OH)_5 + 2FeCl_3 + Ca(OH)_2 + 6Ca(HCO_3)_2 \rightarrow \\ &2(C_5H_{12}ON^+)_n + 2OH^- + 2Fe(OH)_3 + 4Al(OH)_3 + 5CaCl_2 + 10CO_2 + 2CaCO_3 + 2H_2O \end{aligned} \tag{4}$$

The reaction invariants (4) are $[(C_5H_{12}ON^+)_n]$, $[Al^{3+}]$, $[Fe^{3+}]$, $[Ca^{2+}]$, $[H^+]$, $\left[HCO_3^-\right]$, $[OH^-]$, $\left[SO_4^{2-}\right]$and $\left[CO_3^{2-}\right]$. However, $\left[SO_4^{2-}\right]$ and $\left[CO_3^{2-}\right]$ions present in the system do not take part in the neutralisation reactions. Therefore, the electroneutrality equation of the reaction for equation (4) is expressed as :

$$\left[\left(C_5H_{12}ON^+\right)_n\right] + \left[Al^{3+}\right] + \left[Fe^{3+}\right] + \left[Ca^{2+}\right] + \left[H^+\right] = \left[HCO_3^-\right] + \left[OH^-\right] \tag{5}$$

Rewriting (5) gives :

$$\left[HCO_3^-\right] - \left[\left(C_5H_{12}ON^+\right)_n\right] - \left[Al^{3+}\right] - \left[Fe^{3+}\right] - \left[Ca^{2+}\right] = \left[H^+\right] - \left[OH^-\right] \quad (6)$$

Let the difference of the ionic concentrations be expressed as :

$$X = \left[HCO_3^-\right] - \left[\left(C_5H_{12}ON^+\right)_n\right] - \left[Al^{3+}\right] - \left[Fe^{3+}\right] - \left[Ca^{2+}\right] \quad (7)$$

Where

$$X = [H^+] - [OH^-] \quad (8)$$

Assuming that there is perfect mixing in the tank reactor, the relationship between the ionic concentrations of the effluent and input concentrations using the material balance equations can be expressed as :

$$V\frac{d\left[(C_5H_{12}ON^+)_n\right]}{dt} = \left[\left(\left(C_5H_{12}ON^+\right)_n\right)_{in}\right] q_a - \left[\left(C_5H_{12}ON^+\right)_n\right] q_{out} \quad (9)$$

$$V\frac{d\left[Al^{3+}\right]}{dt} = \left[Al_{in}^{3+}\right] q_a - \left[Al^{3+}\right] q_{out} \quad (10)$$

$$V\frac{d\left[Fe^{3+}\right]}{dt} = \left[Fe_{in}^{3+}\right] q_b - \left[Fe^{3+}\right] q_{out} \quad (11)$$

$$V\frac{d\left[Ca^{2+}\right]}{dt} = \left[Ca_{in}^{2+}\right] q_c - \left[Ca^{2+}\right] q_{out} \quad (12)$$

$$V\frac{d\left[HCO_3^-\right]}{dt} = \left[HCO_{3\ in}^-\right] q_{in} - \left[HCO_3^-\right] q_{out} \quad (13)$$

Where $\left[(C_5H_{12}ON^+)_n\right]$ is the polyamine ionic concentration at the mixing tank outlet, $\left[\left((C_5H_{12}ON^+)_n\right)_{in}\right]$ the polyamine ionic concentration at the mixing tank inlet, $[Al^{3+}]$ is the aluminium ionic concentration at the mixing tank outlet, $\left[Al_{in}^{3+}\right]$ aluminium ionic concentration at the mixing tank inlet, $[Fe^{3+}]$ is the ferric ionic concentration at the mixing tank outlet, $\left[Fe_{in}^{3+}\right]$ ferric ionic concentration at the mixing tank inlet, $[Ca^{2+}]$ calcium ionic concentration at the mixing tank outlet, $\left[Ca_{in}^{2+}\right]$ calcium ionic concentration at the mixing tank inlet, $\left[HCO_3^-\right]$ bicarbonate ionic concentration of the effluent stream, $\left[HCO_{3,in}^-\right]$ bicarbonate ionic concentration of influent stream, q_a flow rate of sudfloc 3835 solution, q_b flow rate of ferric chloride solution, q_c flow rate of hydrated lime, q_{out} flow rate of the effluent stream, q_{in} flow rate of the influent stream, V volume of mixing tank, $[H^+]$

hydrogen ions concentration, $[OH^-]$ hydroxide ions concentration and k_m dissociation constant of water.

Adding (9) to (12) and then subtract the sum from (13) gives :

$$\begin{aligned} V\frac{d\left[HCO_3^-\right]}{dt} - V\frac{d\left[\left(C_5H_{12}ON^+\right)_n\right]}{dt} - V\frac{d\left[Al^{3+}\right]}{dt} - V\frac{d\left[Fe^{3+}\right]}{dt} - V\frac{d\left[Ca^{2+}\right]}{dt} = \left[HCO_{3\ in}^-\right] q_{in} - \\ \left[\left(\left(C_5H_{12}ON^+\right)_n\right)_{in}\right] q_a - \left[Al_{in}^{3+}\right] q_a - \left[Fe_{in}^{3+}\right] q_b - \left[Ca_{in}^{2+}\right] q_c + \\ \left[\left(C_5H_{12}ON^+\right)_n\right] q_{out} + \left[Al^{3+}\right] q_{out} + \\ \left[Fe^{3+}\right] q_{out} + \left[Ca^{2+}\right] q_{out} - \left[HCO_3^-\right] q_{out} \end{aligned} \tag{14}$$

The material balance expression of the mixing tank reactor yields :

$$V\frac{dX}{dt} = \left[HCO_{3\ in}^-\right] q_{in} - \left[\left(\left(C_5H_{12}ON^+\right)_n\right)_{in}\right] q_a - \left[Al_{in}^{3+}\right] q_a - \left[Fe_{in}^{3+}\right] q_b - \left[Ca_{in}^{2+}\right] q_c - X.q_{out} \tag{15}$$

Thus, (4.15) is expressed as :

$$V\frac{dX}{dt} = \left[HCO_{3\ in}^-\right] q_{in} - \left(\left[\left(\left(C_5H_{12}ON^+\right)_n\right)_{in}\right] + \left[Al_{in}^{3+}\right]\right) q_a - \left[Fe_{in}^{3+}\right] q_b - \left[Ca_{in}^{2+}\right] q_c - X.q_{out} \tag{16}$$

The dissociation equation for water is

$$\left[H^+\right].\left[OH^-\right] = k_w = 10^{-14} \tag{17}$$

Substituting (8) into (17) gives a quadratic expression :

$$[H^+]^2 - X\left[H^+\right] - k_w = 0 \tag{18}$$

The solutions of the equation (4.18) are written as :

$$\begin{aligned} &\text{If } X > 0, \text{ then } [H^+] = \tfrac{X+\sqrt{X^2+4k_w}}{2} = \tfrac{X}{2}.\left(\sqrt{1+\tfrac{4k_w}{X^2}} - 1\right) \\ &\text{If } X = 0, \text{ then } [H^+] = \sqrt{k_w} \\ &\text{If } X < 0, \text{ then } [H^+] = \tfrac{X-\sqrt{X^2+4k_w}}{2} = -\tfrac{X}{2}.\left(\sqrt{1+\tfrac{4k_w}{X^2}} + 1\right) \end{aligned} \tag{19}$$

The concentration of the hydrogen ions $[H^+]$ may be expressed in the logarithmic function as :

$$pH = -\log\left[H^+\right] \tag{20}$$

The expression for the surface charge of the raw waters is obtained as described in section 3.1.

$$\sigma = \left[(2/\pi)\, n\varepsilon\kappa T\right]^{1/2} \sinh 1.15\,(pH_0 - pH) \tag{21}$$

Where σ is the surface charge , κ is the Boltzmann constant, T is the temperature, ε refers to the relative dielectric permittivity, pH_0 PH at point of zero charge and n ionic strength.

From (12), (20) and (21), the dynamics of the chemical dosing unit is formulated. The surface charge and pH are the controlled output variables while the coagulant flow rate (q_a), co-coagulant flow rate (q_b) and pH adjustment chemical flow rate (q_c) are the control input variables of the model.

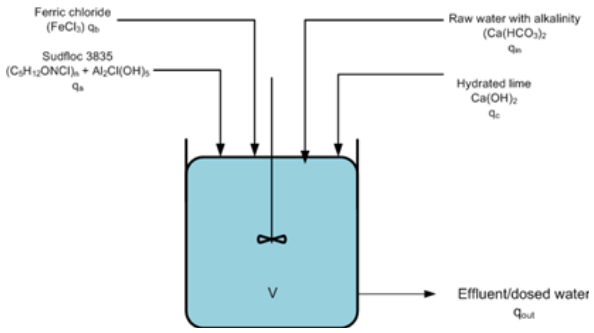

Fig. 2 – Mixing tank reactor for the coagulation chemical dosing unit.

2.3. Identification with Wiener models

Wiener model consists of a linear dynamic system G followed by a static nonlinearity f as shown in Fig. 3. The input u and the output y are measurable, while the states of the models are denoted by x which can be observed. For the linear dynamic system of the Wiener model structure, it could be written as :

$$x\,(t) = G\,(q, \theta)\, u\,(t) \tag{22}$$

Similarly, the nonlinearity part is expressed as

$$y\,(t) = f\,(x\,(t)\,, \eta)\, u\,(t) \tag{23}$$

By combining (22) and (23) together, the output of the Wiener model structure is :

$$y\,(t) = f\,(G\,(q, \theta)\, u\,(t) + v\,(t)\,, \eta) + e\,(t) \tag{24}$$

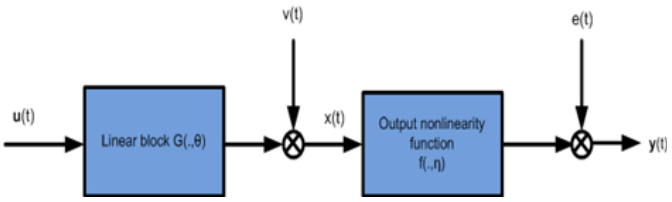

Fig. 3 – Wiener model structure.

The linear dynamic system that shows the relationship between the input and the output could be represented in the discrete state-space form as [10] :

$$\begin{aligned} \xi(k+1) &= A\xi(k) + Bu(k) \\ y(k) &= C\xi(k) + Du(k) \end{aligned} \tag{25}$$

where ξ is the state vector, consisting of n state variables. a, B and C are system matrices. The nonlinear block is static and thus a real-valued function of the state variables. The general structure of the nonlinear block can be expressed using the function expansion with basis functions and parameters :

$$y = \sum_{i=1}^{n_b} f_i B_i(x) \tag{26}$$

where $B_i(x)$ is the basis function. The commonly used basis functions for the nonlinear blocks are :

Power Series :

$$B_i(x) = x^i \qquad i = 0, 1, 2 \ldots, n_b \tag{27}$$

where n_b is the number of input time steps.

Chebyshev polynomials :

$$B_j(x_j) = \begin{cases} 0 & if \quad (x \leq x_{i-1}) \\ \left(\frac{x - x_{i-1}}{x_i - x_{i-1}}\right) & if \quad (x_{i-1} \leq x \leq x_i) \\ \left(\frac{x_{i+1} - x}{x_{i+1} - x_i}\right) & if \quad (x_i \leq x \leq x_{i+1}) \\ 0 & if \quad (x_{i+1} \leq x) \end{cases} \tag{28}$$

Piecewise polynomial :

$$B_k = \frac{1}{1 + e^{-\left(\eta_{o_k} + x\eta_{1_k}\right)}} \tag{29}$$

where η_{o_k} and η_{1_k} are internal parameters of the sigmoid function that determines the position of the transition from 0 to 1 and how fast.

Wavelets :

$$B_{i,j}(k) = \frac{1}{\sqrt{2^i}}\psi\left(\frac{x - 2^i j}{2^i}\right) \tag{30}$$

where i is a scaled parameters, j is the dilation parameter and y is the mother wavelets.

The goal of identification using Wiener model is to estimate the two parameters, θ and η, using the measurements of the input u and the output y to achieve the best model for the process under consideration. When the parameters θ and η, and the given input u are known, then the predicted output, $\hat{y}(k, \theta, \eta)$ could be estimated. In order to estimate the quality of a model, the predicted output $\hat{y}(k)$ and measured output y are compared using a prediction error criterion. The prediction error criterion for this purpose is stated as :

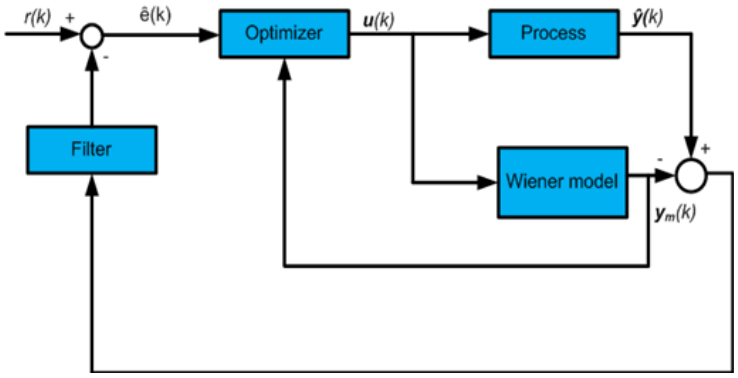

Fig. 4 – Block diagram of WMPC scheme.

$$V_N(\theta, \eta) = \frac{1}{N}\sum_{k=1}^{N}\left(y(k) - \hat{y}(k, \theta, \eta)\right)^2 \tag{31}$$

where N is the number of data.

The implication of (31) is that the best model has the minimal value of $V_N(\theta, \eta)$ which depends on the optimal estimate of these two parameters [10].

2.4. Wiener model predictive control scheme

MPC scheme based on the Wiener model is presented in this study. MPC basically uses the dynamic model of the plant to predict and optimise the future behaviour of the process. At each control interval, the MPC algorithm computes a sequence of future input control moves over a control horizon M, in order to optimise the future response of the plant. The optimisation of the plant behaviour is achieved by minimising an objective function based on a desired output trajectory over a prediction horizon P. Only the first value of the input control move sequence is applied into the plant others are discarded,

then the horizon is moved one step towards the future, and the optimisation process is repeated. The objective function can be written as :

$$J = \sum_{i=0}^{P} \left\| \hat{y}_{k+i|k} - r_{k+i} \right\|_{Q(i)}^{2} + \sum_{i=0}^{M-1} \left\| u_{k+i|k} \right\|_{S(i)}^{2} + \sum_{i=0}^{M-1} \left\| \Delta u_{k+i|k} \right\|_{R(i)}^{2} \tag{32}$$

where $\hat{y}_{k+i|k}$ represents the prediction, made at time k, of the output at time $k+i$, r_{k+i} is the value of the reference at time $k+i$ and $u_{k+i|k}$ and $\Delta u_{k+i|k}$ are the control input and control input increment, computed at time k, at time $k+i$ respectively. $Q(i)$, $S(i)$ and $R(i)$ are positive semi-definite diagonal weighting matrices, and $\|x\|_{w} = \sqrt{x^{T} W x}$ is the weighting 2-norm of vector x. The prediction horizon P, control horizon M, the weighting matrices are design parameters of the MPC that are tuned to obtain desired performances.

In formulating the MPC algorithm, constraints on the process due to the limited range and dynamic response of actuators, operational, safety, economic or environmental factors are taking into consideration. The constrained optimisation problem solved in the MPC algorithm is stated as [8] :

$$\underbrace{\min}_{\Delta u} J(k) \tag{33}$$

subject to :

$$\begin{aligned} & u_{\min}^{i} \leq u_{k}^{i} \leq u_{\max}^{i} \\ & \Delta u_{\min}^{i} \leq \Delta u_{k}^{i} \leq \Delta u_{\max}^{i} \\ & y_{\min}^{i} \leq y_{k}^{i} \leq y_{\max}^{i} \end{aligned} \tag{34}$$

where i represent the ith component of the corresponding vector. The WMPC scheme in Fig. 4 is implemented by using the identified Wiener model as a replacement for the internal model employed in the standard MPC algorithm for predicting the future response and optimisation.

Table 1 – Process modelling variables.

Variable	**Symbols**	**Values and units**
Polyamine and aluminium ions concentration	$[(C_5H_{12}ON^+)_n + [Al^{3+}]]$	0.0001 mol/L
Ferric ions concentration	$[Fe^{3+}]$	0.0001 mol/L
Calcium ions concentration	$[Ca^{2+}]$	0.0001 mol/L
Bicarbonate ion concentration	$\left[HCO_3^-\right]$	0.0001 mol/L
Hydrogen ion concentration	$[H^+]$	10^{-7} mol/Litre
Coagulant flow rate	q_a	0.14 Litres/s
Hydrated lime flow rate	q_b	0.7 Litres/s
Influent water flow rate	q_{in}	462.96 Litres/s
Tank Volume	V	8000 Litres
Dissociation constant of water	K_w	10^{-14}
Temperature	T	298 K
electron charge	e	1.6×10^{-19} C
Ionic strength	n	50×10^6 mol/cm3
Relative dielectric permittivity	ε	80
Boltzman constant	κ	$1.38\times10^{23} JK^{-1}$
Faraday constant	F	96,490 Ceq^{-1}
Universal gas constant	R	8.314 $Jmol^{-1}K$

3. Results and discussions

3.1. Simulation model results

The simulation model of the coagulation chemical dosing unit described in the previous section was developed and simulated in MATLAB 7.10 environment. The simulation parameters are stated in Table 1. The input variables to the simulation models were the data collected from the water treatment plant for a period of 690 days. The response of the simulation model is presented in Fig. 5.

The simulation results show that surface charge values are within the range of $-1 \times 10^{-5}\mu eq/mg$ and $+7 \times 10^{-5}\mu eq/mg$ and the pH values fall between the range of 7 and 8.5. Based on these results, a suitable control scheme is proposed for the dosing unit to ensure that its output variables follow the desired set-points.

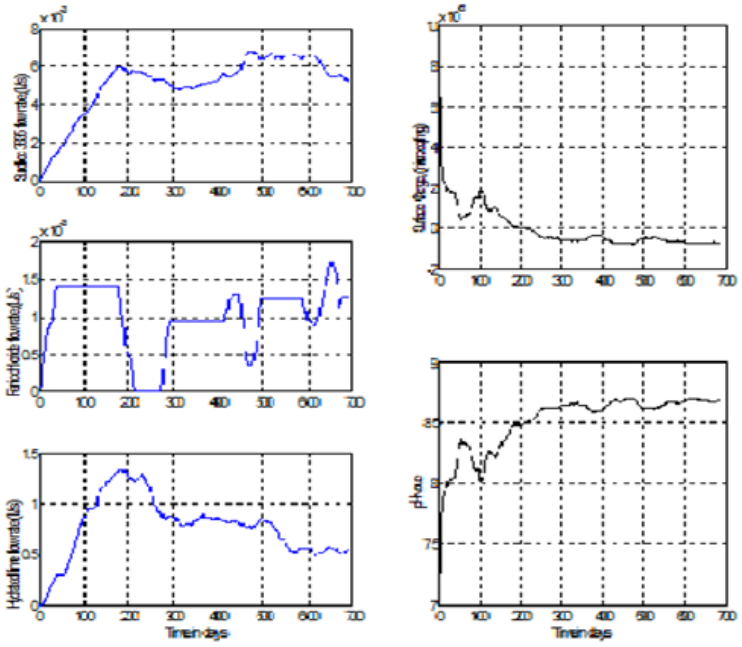

Fig. 5 – Input and output datasets.

3.2. Performance of the estimators

The following four nonlinearity blocks were used in the Wiener model for the system identification of the coagulation process : piecewise linear, polynomial, sigmoid, and wavelet network. The results of each nonlinear block are compared with each other and the measured output data of the dosing unit. The estimation results of the nonlinear blocks are shown in Fig. 6. It is observed from the results that the wavelet network had the highest goodness of fit and hence the best estimators among them. In view of this finding, the wavelet estimator is thus used as nonlinear estimator for the Wiener model of the process.

3.3. Performance of the WMPC scheme

The WMPC scheme proposed in the previous section was implemented using the MPC toolbox in the MATLAB 7.10/Simulink software. Simulation constraints were placed on the manipulated variables to take into consideration the minimum and maximum flow rate of the metering pumps discharging the sudfloc 3835 (q_a), secondary coagulant (q_b) and hydrated lime (q_c) into the rapid mixing tank. A lower limit of 0 L/s and an upper limit of 2 L/s were selected for these variables. The prediction horizon, was chosen as P = 15, while the control horizon as M = 5. Each of weighting matrices S, R and Q was selected as diag (0.1,0.1,0.1).

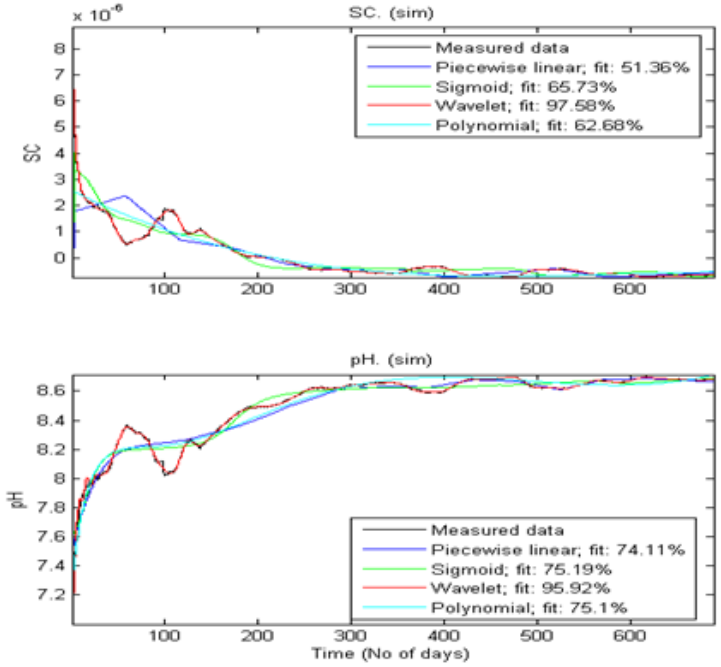

Fig. 6 – Comparison of the nonlinear estimators/functions with the measured output dataset.

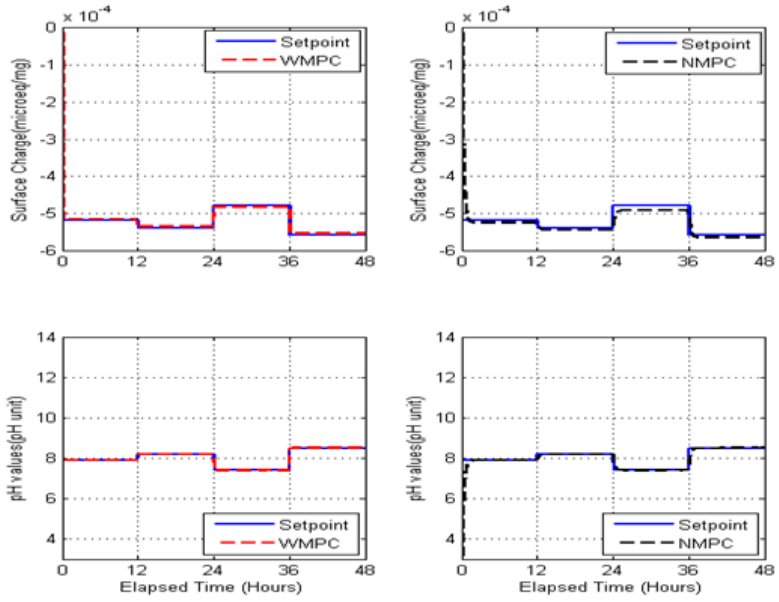

Fig. 7 – Set point tracking performance.

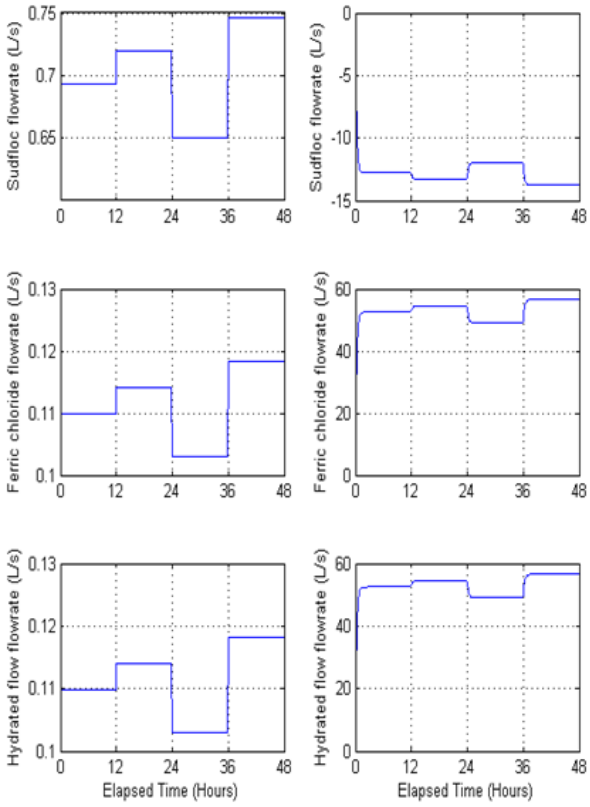

Fig. 8 – Control input moves.

In the first simulation experiment, the response of WMPC scheme to changes in the reference trajectory was examined. The system was simulated for a period of 48 hours while the set points were changed every twelve hours. The simulations results of the WMPC compared with the nonlinear model predictive control(NMPC) scheme are shown in Fig. 7. It can be observed that the WMPC scheme tracks the reference trajectory satisfactorily and its normalised root mean square error (RMSE) values in Table 2 are lower than that of NMPC. Fig. 8 shows the control input moves to achieve the set-point tracking performance of the two control schemes. The performance of the WMPC scheme when the system is subjected to disturbances in form of input and output noise signals and step signals on the manipulated input channels was investigated in the second simulation experiment. The simulation results when compared with the NMPC are shown in Fig. 9. The control input moves of the control schemes are shown in Fig. 10. The WMPC scheme behaved appropriately by rejecting the disturbances acting on the system without violating the constraints placed on the manipulated variables. In addition, the normalised RMSE values of WMPC are smaller than that of NMPC indicating a better performance of WMPC over NMPC.

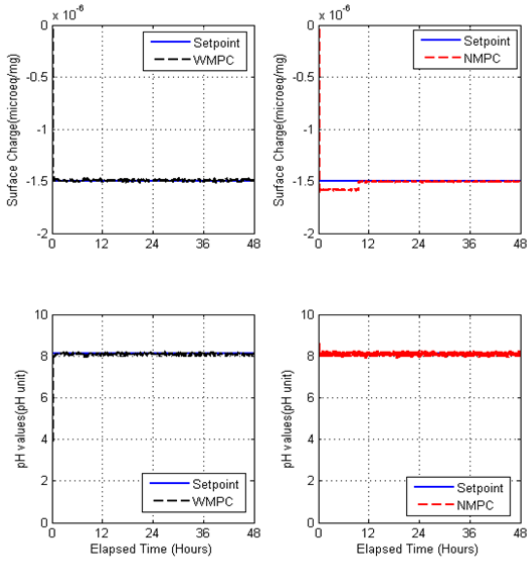

Fig. 9 – Noise and disturbance rejection performance.

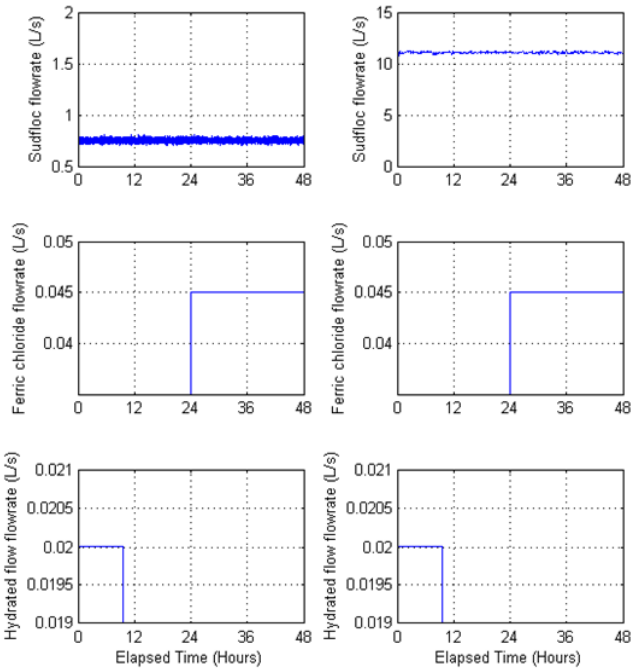

Fig. 10 – Control input moves.

Table 2 – .

Control scheme	Surface Charge (SC)	pH
WMPC(Setpoint)	0.01085	0.1495
NMPC(Setpoint)	0.02880	0.4254
WMPC(Disturbance)	0.03919	0.1335
NMPC(Disturbance)	0.04559	0.2421

Conclusion

The study has presented the Wiener model identification and predictive control of coagulation process in the water treatment plants. Input-output data from the simulation mode developed using the mechanistic modelling tech niques were applied for the identification of the Wiener models of the coagulation chemical dosing unit. A comparison of the different Wiener models evaluated in the study showed that the Wiener model based on Wavelet network block had the best prediction capabilities. This Wiener model was thus proposed as the internal model of MPC algorithm instead of a standard linear model. Simulation results showed that the proposed Wiener based MPC algorithm could effectively handle the coagulation process control in water treatment operations. In continuation of this study, the subspace model identification may be examined and compared to the wavelet model identification technique. In addition, the use of genetic programming and other evolutionary computational modelling techniques could be investigated and applied in conjunction with the predictive control for coagulation process.

Acknowledgement

This research was supported by the Tshwane University of Technology, Pretoria, South Africa. Our special thanks go to Dr. M.A. Kazaure for his useful suggestions. Our profound gratitude to the Management and Staff of Rietvlei Water Treatment plant, City of Tshwane, for their cooperation in respect of this study

REFERENCES

[1] A. Adgar, C.S. Cox and C.A. Jones. Enhancement of coagulation control using the streaming current detector. Bioprocess Biosystem Engineering, 27 :349–357, 2005.

[2] C.W. Baxter, Q. Zhang, S.J. Stanley, R.R. Shariff, T. Tupas, and H.K. Stark. Drinking water quality and treatment : The use of artificial neural networks.Canadian Journal of Civil Engineering, 28 :26–35, 2001.

[3] C.W. Baxter, R. Stanley, Q. Zhang, and D.W. Smith. Developing artificial neural network models of water treatment processes : A guide for utilities. Journal of Engineering Science, 1 : 201–211, 2002.

[4] O. Bello, Y. Hamam and K. Djouani. Modelling of a coagulation chemical dosing unit for water treatment plants using fuzzy inference system. Proceedings of the 19th World Congress of the International Federation of Automatic Control, Cape Town, 3985–3991, 2014.

[5] O. Bello, Y. Hamam and K. Djouani. Modelling and validation of a coagulation chemi-

cal dosing unit for water treatment plants. Proceedings of the IEEE Multi-Conference on System and Control, Antibes, France, 765–771, 201

[6] V.P. Evangelou. Environmental soil and water chemistry : Principles and applications. John Wiley, New York, 1998.

[7] I. Fletcher, A. Adgar, C.S. Cox, M. Johnson, T. Pearson and A. Wetheril. Optimal coagulation control issues at surface treatment works : problems and a new solution. Proceedings of the 10th Mediterranean Conference on Control and Automation, Lisbon, 2002.

[8] J.C. Gomez, A. Jutan and E. Baeyens. Wiener model identification and predictive control of a pH neutralisation process. IEE Proc. Control Theory Appl., 151(3) : 329-338, 2004.

[9] T. Han, E. Nahm, K. Woo and J. Ryu. Optimisation of coagulation dosing process in water purification system. Proceedings of the 36th SICE Annual Conference, Tokushima, 1105–1109, 1997.

[10] A. Hagenblad. Aspects of the identification of Wiener models. PhD thesis, Linkopings Universitet, 1999.

[11] S. Heddam, A. Bermad, and N. Dechemi. ANFIS-based modelling for coagulant dosage in drinking water treatment plant : A case study. Environmental Monitoring and Assessment Journal, 184 :1953–1971, 2012.

[12] J.R. Jang. ANFIS : Adaptive-network-based fuzzy inference system. IEEE Transactions on Systems, Man and Cybernectics, 23 :665–685, 1993

[13] A. D. Kalafatis , L. Wang and W. R. Cluett, Identification of Wiener type nonlinear systems in a noisy environment, International Journal of Control, 66 :(6)923–941, 1997.

[14] S J. Norquay, A Palazoglu, and J A Romagnoli, Application of Wiener Model Predictive Control (WMPC) to a pH Neutralization Experiment, IEEE Transactions on Control Systems Technology, 7(4) :437–445, 1999.

[15] R.F. Olanrewanju, S.A. Muyibi, T.O. Salawudeen, and A.M. Aibinu. An intelligent modelling of coagulant dosing system for water treatment plants in artificial neutral networks. Australian Journal of Basic and Applied Sciences, 6 : 93–99, 2012.

[16] S. Vijayachitra, A. Tamilarasi and M.P. Kumar. Multiple input multiple output (MIMO) process optimisation using fuzzy GA clustering. International Journal of Recent Trends in Engineering, 2 :16–18, 2009.

[17] G. Wu and S. Lo. Predicting real-time coagulant dosage in water treatment by artificial neural network. Engineering Applications of Artificial Intelligence, 21 : 1189–1195, 2008.

[18] H. Zhang and D. Luo. Application of an expert system using neural network to control the coagulant dosing in water treatment plant. Journal of Control Theory and Applications, 2 : 89–92, 2004.

p-ISSN : 2335-1357 e-ISSN : 2437-1122

Mediterranean Journal of Modeling and Simulation

Med. J. Model. Simul. 05 (2016) 046-058

Design and analysis of gasket cutting machine

Vipin V. Gopal [a] *, Lokavarapu Bhaskara Rao [a]

[a] School of Mechanical and Building Science, VIT University, Chennai Campus, Vandalur-Kelambakkam Road, Chennai, Tamil Nadu, India

ARTICLE INFO

Article history :
Received October 2015
Accepted February 2016

Keywords :
Gasket ;
Fully automated ;
Idealization of system ;
Cost analysis ;
Design for manufacturing and assembly.

ABSTRACT

Paper is about the design and analysis of the optimized gasket cutting machine which can be provide to the companies where there is use of gaskets at a certain interval of time. The paper contain the cost optimized machine which is provide at a much lower cost as compared to the machines presently available in the market. This machine can be specifically used for the boiler and refrigeration companies where the gaskets are used to avoid the leakage due to the joining of two different diametric pipes. Inspite of giving a large order of gaskets, they can prepare the same at small rate whenever needed at the location.

1. Introduction

Gasket is a mechanical seal that is used for filling the space between two surfaces, usually to prevent the leakage between the two objects which is under compression. Gaskets are used to cover irregularities on mating surfaces of machine parts. They are commonly produced by cutting from sheet materials such as paper, rubber, silicon, metal, fiber and asbestos lining material (L. Angrisani et al, 1999).

The use of gaskets in automobiles, chemical plants, power plants, ship building yard, breweries, dye, stuff plants, oil refineries, refrigeration plants, allied industries, assembly lines in refrigeration plants etc (Trelleborg sealing solution,2011). In refrigeration and air conditioning system during assembly of the pipes different diameters pipes are bolted together (David A. Nash et al, 2009; Dennis R. Moss et al, 2012). During joining the two different diameters pipe there is a possibility of leakage due to improper contact between them. During assembly there is a major problem of leakage of refrigerant leads to decrees the internal pressure and flow rate of refrigerant. These gaskets get degraded after a specific life time. And for the replacement the companies have to order the same in a bilk. So, rather than buying the gasket the company can have one of the machines so that they can make the gasket whenever needed. But in market the gasket machine

*Email : bhaskarbabu_20@yahoo.com

is available at 30,000-50,000 INR (471- 785 USD). In this paper design of the machine which can cuts gasket rings of different diameters as per requirement.

The machine can be operated manually and can be designed to cut gasket of different diameters and sizes with proper accuracy of +/- 1mm by using this special purpose machine the gasket rings of different diameters can be cut and used in assembly line. The gasket sheets up to 3mm to 5 mm thickness can be cut with proper accuracy. The machine doesn't require any kind of external supply. It doesn't need electric power to run, so it can be used in remote area also. Or otherwise the machine can be operated manually, semi-automated or fully automated depending upon the need. The machine is portable and simple in working.

2. Numerical modeling

Designing is the process of developing a product followed by generation and evaluation of the same. The designing process includes identification, refining, evaluating and then the documentation of the designed product. The design procedure is well depicted in Figure 1.

Fig. 1 – Design procedure.

2.1. Design consideration

For the designing of the gasket cutting machine it was necessary to assign some constant parameters for the initial designing procedure (James Walker Moorflex). So, for the same in this paper the diametric range of the gasket ring is considered to be 50mm to 300mm and an accuracy of +/- 1mm. The maximum thickness of the gasket sheet is considered to be 5mm. The length of the guide way is 700mm and height of the machine is 250mm. The main factor of consideration is the ovality ; there should be no ovality error.

2.1.1. Design and description of the different components

The machine consist of base frame subassembly that contains L-angle guide ways on which disk can be slide the supporting panel of the machines that are front supporting plates and L-shaped plates to support the total weight of machine and hold it at proper ground clearance (M.F. Spotts et al, 2011).

Another sub assembly contains the supporting disk with its mountings. On the guide ways the sliding support can be fixed which can slides the disk as per requirement. Above that the disk holder can be placed which holds the disk in proper manner. On which the disk is mounted which both can have sliding as well as rotating motion due to arrangement of bearing. To hold the gasket in proper position above the disk the ovality reducer is placed which can be fitted by screw and thread arrangement.

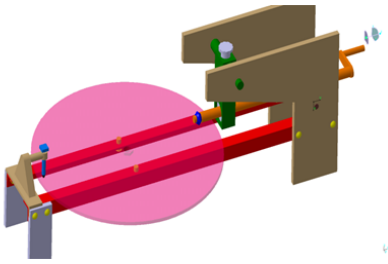

Fig. 2 – Design model of the gasket cutting machine (Catia User Manual).

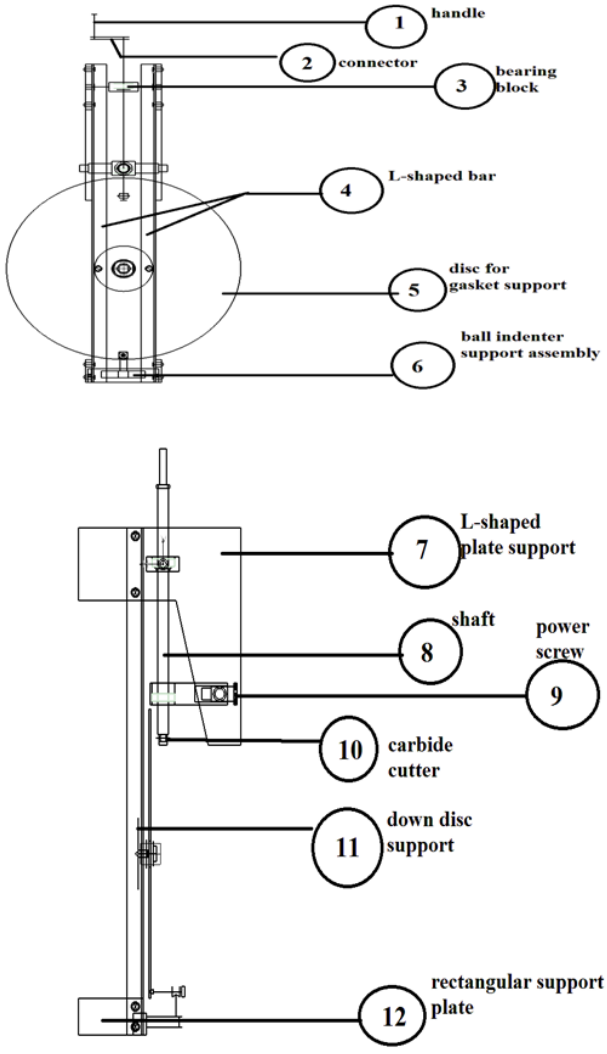

Fig. 3 – Schematic model of gasket cutting machine.

There is another arrangement of roller which can also sides along disk on guide ways with disk. It helps to support the disk at the load side to reduce its tilting effect towards the load side. The cutting operation can be done by carbide tip cutter mounted on the

solid shaft at its end. Which can be pressurized by the nut and screw arrangement its head. The shaft is pivoted at one support close to its other end. It consists of handle which can used to rotate the shaft. By simply rotating it the cutting operation can be done. The design model of the gasket cutting machine is shown in Figure 2.

The gasket cuttig machine was modeled taking into consideration, the conventional geomerty of the model. The new characterestics was achieved by introducing an innovative idea of reducing the number of parts and reducing the complexity of the design by using a simple design. The nuber of parts used is less as compared to the previous design. The concepts of design for manufacturing and assembly is been greatly used. The circular base 10 for mounting the raw material is made more dynamically sound by applying necessary constraints.

The constrains can be added or removed according to the work application. To avoid the sagging or bukling of the raw material during cutting a ball indenter support 11 is provided. This innovative design lets the new design to stand out of the crowd because of its uniqueness. FIG. 3 shows the respective view of the gasket cutting machine consist of two L-angle bars 4 which is supported by L shaped plates 7 on one end and rectangular shaped plate 12 on other end. These ensures the stability of the parts above the L-angle bar and provide a good support to the system.

The front frame according to the embodiment includes a ciruclar disc plate 5 on the bars on which the raw materials kept inorder to cut gaskets. These are attached to the bars with the help of the disc support 11 which is tightend with the help of screw. Now a shaft 2 is used in which to the end the carbide tool 10 can be fixed which is useful for cutting the gasket. To the other end of the shaft consist a handel 1 which makes it useful during the period of power cuts. The gasket cand me cut by rotating the handel too.

This shaft is held in a position by using two blocks ; one is bearing block 3 and another one is couple block . These two consists of bearing house which enhances the easy rotation of the shaft. Figure also shows couple block which contains a power screw 9 which provides or which is used to maintain the essential pressure needed to cut the gasket. By rotating the power screw we can change the pressure because as we rotate the screw it pressurises the shaft to bend thus applying pressure on the gasket material.

The assembly consisting of the ball indenter which is used to provide an essential reaction or support to the gasket material to avoid sagging or bending of material due to the application of force by the cutter. To the bottom a shaft or pulley is attached to the disc down support 11 through which a belt is attached which is inturn connected to the motor which can be used to rotate the disc which will appreciate the use of automatic cutting of gasket. The shaft consisting of the tool can be moved linearly to adjust the diameter of the gasket that is to be made.

3. Analysis

The next step after designing is to do the analysis of the product. In earlier days, for analysis one has to actually make a prototype which is actually a very lengthy process and waste of time. But the modern technology has provided the easy way of analyzing the design with the help of software's. Analysis is an essential process as it helps in determining the major failure parts of the system under study. The use of software's has

made it easy to check the actual failures same as if the design would have been subjected to the actual working conditions. For the analysis using software's one has to idealize the system geometry, field conditions, boundary conditions etc and the results so obtained from the analysis are next to accuracy and it will or may differ from other software's as the solvers used by the software way differ. The results may differ but the difference in the results will be very less.

3.1. Mesh

The analysis of the system was carried out using Ansys software. For the analysis to start it is very important to mesh the design which has been imported. Meshing is the process of discretizing the model into small distinct parts. Finer the mesh more accurate will be the result. The meshing used is the tetrahedral mesh and the meshing is shown in Figure 4.

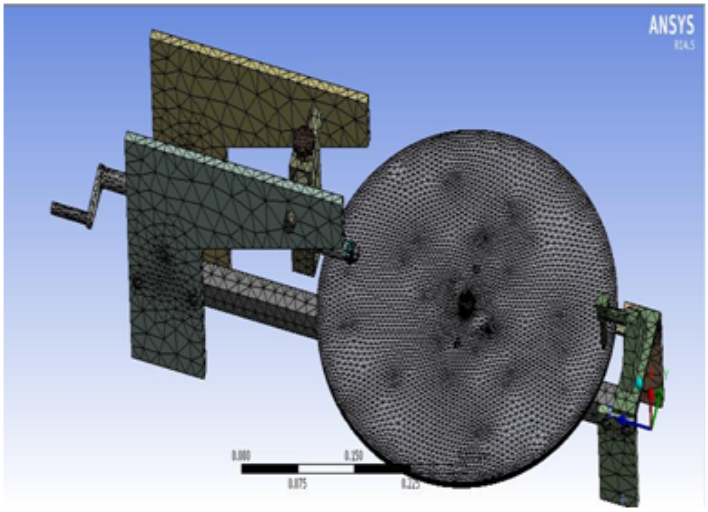

Fig. 4 – Meshing of the designed part (Ansys workbench).

The respective number of nodes and elements generated is shown in Table 1. As the mesh count increases there is an increase in number of nodes and element.

Table 1 – Shows the number of element and node obtained in meshing (Ansys workbench).

Statistics	
Nodes	124043
Element	62990
Mesh metric	None

After doing the meshing it is necessary to give essential boundary conditions such as the end conditions, forces moment etc to get the accurate result (Koji Teramoto et al, 1998 ; Edgar R., 2012). The boundary conditions applied to system are ; a pressure of 398

Pa is applied on the plate due to cutter, a reactant force of 50 N is applied by the ball indenter support, and legs of the system are fixed. The boundary conditions fed to the software is shown in Figure 5.

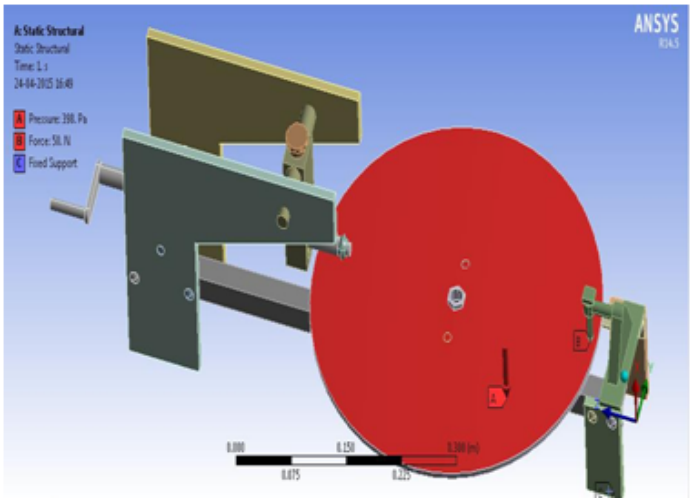

Fig. 5 – Boundary condition given to the design (Ansys workbench).

The values of the forces applied to the model as shown in Figure 5 are given in the Table 2.

Table 2 – Values of the boundary condition applied to the model (Ansys workbench).

Object name	Pressure	Force	Fixed support
State	Fully defined		
Scope			
Scoping method	Geometry selection		
Geometry	1 face	2 face	3 face
Definition			
Type	Pressure	Force	Fixed support
Define by	Component		
Coordinate system	Global coordinate system		
X component	-398 Pa (ramped)	-50 N (ramped)	
Y component	0 Pa (ramped)	0 N (ramped)	
Z component	0 Pa (ramped)	0 N (ramped)	
Suppressed	No		

3.2. Results

After giving the all the essential boundary conditions and running for the results. The first is the deformation result, it is found that the maximum deformation obtained is 0.004 mm which is a very small deflection and can be neglected. The following deflection is shown in Figure 6.

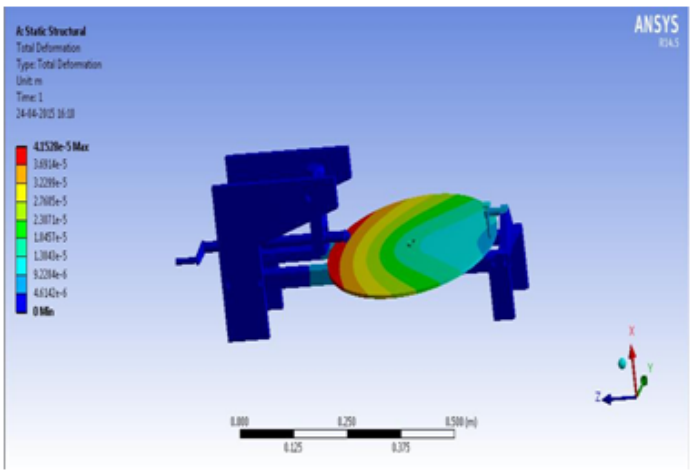

Fig. 6 – Deformation of the designed model (Ansys workbench).

The maximum value of stress induced in the designed model is 1.6765e7 Pa; whereas the maximum allowable stress for the model is 2.5e8 Pa. Thus, the model is safe as per stress point of view and is shown in Figure 7.

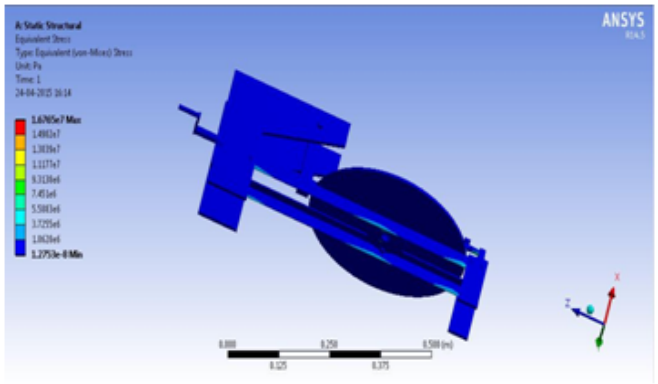

Fig. 7 – Von-Mises stress analysis of the designed model (Ansys workbench).

Similarly, the maximum value of strain subjected to the model is 9.3733e-5 m/m, while the actual value is 4e-6 m/m. Thus the model is safe and is shown in Figure 8.

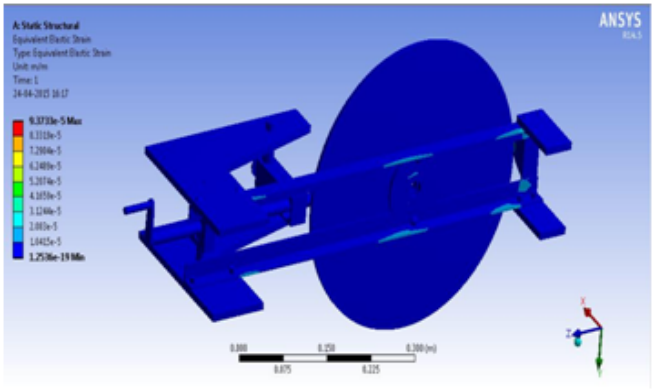

Fig. 8 – Von-Mises strain analysis of the designed model (Ansys workbench).

According to the results obtained from the results, the maximum and the minimum values of the desired parameters and the area of effect is shown in Table 3.

Table 3 – Maximum and minimum values of deformation, equivalent stress and strain (Ansys workbench).

Object name	Equivalent stress	Equivalent strain	Total deformation
State	Solved		
Scope			
Scoping method	Geometric selection		
Geometry	All bodies		
Definition			
Type	Equivalent (von-Mises) stress	Equivalent elastic strain	Total deformation
By	Time		
Display time	Last		
Calculate time history	Yes		
Suppressed	No		
Integration Point Result			
Display option	Averaged		
Results			
Minimum	1.2753e-008 Pa	1.2536e-019 m/m	0 m
Maximum	1.6765e+007 Pa	9.3733e-005 m/m	4.1528e-005 m
Minimum occurs on	Shaft		Down support
Maximum occurs on	Gasket indenter		Circular disc

3.3. Idealization of the results

From the results which were obtained from the analysis of the designed model it is clear that the maximum deformation occurs in the disc. Therefore, analysis for the disc alone was done by using Ansys APDL. Both Ansys classical and workbench are used for the analysis purpose but for more theoretical results Ansys classical are used but work

industrial application workbench are used. The same boundary conditions were given for the analysis as it was given during workbench except the fixed support i.e., a pressure of 398 Pa is applied on the plate due to cutter, a reactant force of 50 N is applied by the ball indenter support and the centre of the disc is constrained with all degrees of freedom. The boundary conditions so given are shown in Figure 9.

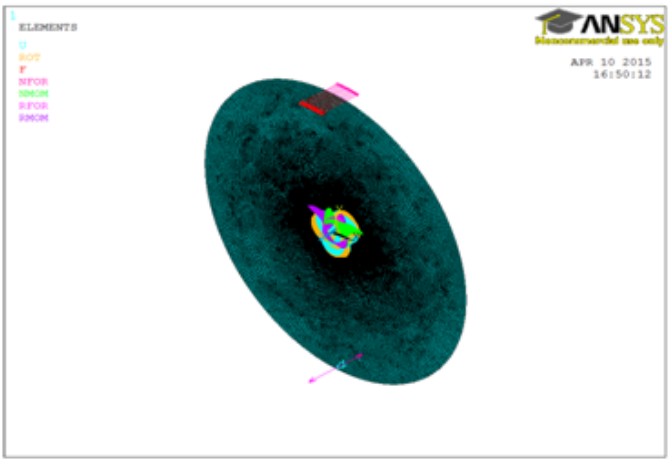

Fig. 9 – Boundary conditions given to the disc (Ansys APDL).

The main concern is with the deformation of the disc. The analysis was carried out and the deformation seemed to be 0.011484 mm which is a negligible value and hence can be neglected. The deformation of the disc is shown in Figure 10.

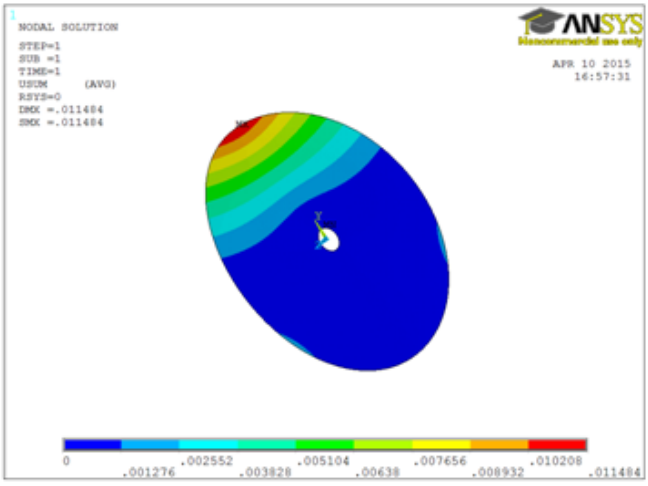

Fig. 10 – Deformation of the disc (Ansys APDL).

The results obtained from both the analysis were satisfying and was well beyond the limits and hence is safe. Thus the structure can be used for the industrial applications.

4. Cost Analysis

In order to sell the product in a market, the product should have enough qualities. One of such factor is the cost (Bryan R. et al, 2011 ; G. Boothroyd et al, 1993). When it comes to the market survival and to compete with the other companies it is necessary that the product should attract the customers and the first factor which attracts the customers is the cost of the product. The products are required to be manufactured at the lower cost and with good qualities.

4.1. Manufacturing methods

The important factor which decides the cost of the part is the cost of machining or different manufacturing process used for manufacturing the respective parts. The manufacturing process of the parts required for the model has been explained in Table 4.

Table 4 – Manufacturing methods of the parts.

Sr.No :	PARTS	PROCESS
1	Shaft	1. Power hacksaw 2. Facing 3. Turning
2	Side plate	1. Gas cutting 2. Grinding 3. Drilling
3	L angle	1. Cutting 2. Grinding 3. Drilling
4	Bearing block	1. Power hacksaw 2. Drilling 3. Boring 4. Turning
5	Nut Block	1. Power hacksaw 2. Drilling 3. Threading 4. Turning
6	Guide way upper plate	1. Power hacksaw 2. Drilling 3.Threading
7	Supporting roller	1. Power hacksaw 2. Drilling 3. Threading 4. Welding
8	Circular disc	1. Gas cutting 2. Drilling

4.2. Cost of manufacturing

The cost analysis of the product is done using DFM software. The calculated cost of the designed model is shown in Table 5.

Table 5 – Cost analysis of the model (DFMA user manual).

Sr. No	PART NAME	MATERIAL	WEIGHT (Kg)	QTY	COST (INR)	COST (USD)
1	M.S Plate	Mild steel	9	2	675	10.6
2	L Angle	Mild steel	2	2	150	2.36
3	Rectangular bar	C45	4	3	300	4.71
4	Nut	Std		23	50	0.78
5	Bolts	Std		25	114	1.79
6	Wicer	Std		1	6	0.09
7	Circlips	Std		5	20	0.31
8	Bearing 6002	Std	0.05	2	305	4.79
9	Bearing	Std	0.025	1	70	1.1
10	Cutter	Std	0.05	1	400	6.28
11	Machining charges				1550	24.33
12	Fabrication charges				1250	19.63
13	Painting				300	4.71
	Total		15.125		5190	81.48

But there is always a scope of reducing the overall cost by eliminating some unnecessary things from the designed model. This can be done by using DFMA software. The assembly reduction analysis result is shown in Table 6.

Thus Table 5 shows that the cost of the designed model can be reduced depending upon the necessity. The weight of the disc can be varied by varying the thickness of the disc. The thickness of the disc will vary upon the type of gasket that has to be cut.

Table 6 – Cost reduction analysis of the assembly (DFMA user manual).

PART NAME	WEIGHT	QTY.	COST	WEIGHT REDUCTION POSSIBLE	COST REDUCTION POSSIBLE
Rectangular bar	4	3	300	2	150
Cutter	0.05	1	400		300
Machining charges			1550		800
Fabrication charges			1250		300
Disc material	4	1	320	3	230
TOTAL	15.125		5190	5 Kg	1780 INR (27.95 USD)

PRODUCT WEIGHT	15.125 - 5 kg	7.7 kg
PRODUCT COST	5190 – 1780	3410/- INR (53.54 USD)

5. Conclusion

As discussed above, the design is fully safe and can be used in the best possible way. Now the industries can create the gasket at the own places without going for other dealers. The designed concluded that the main difference between the existing and the new design model is that the design complexity is reduced so that one can assemble it easily (G. Boothroyd, 2010), the weight of the model is been reduced so thus light in weight and the last but not the least the cost of the product is been reduced to a greater extent. The design can be used manually, semi-automatic or fully automated.

The designed model proves to be much more superior to the existing gasket cutting machine. And by using this system will surely will reduce the dependency of the industry on other gasket producing dealers. The result during the analysis of the project was good which indicate that the product is ready for its application

REFERENCES

[1] Angrisani, L., Daponte, P., Liguori, C., Pietrosanto, A. 1999. An image-based measurement system for the characterization of automotive gaskets. Measurement, Vol.25, No.3, pp.169-181.

[2] Trelleborg sealing solution. 2011. Trelleborg's flat gaskets fulfil a range of different equirements. Sealing Technology, Vol. 2011, No. 5, pp.2.

[3] David A. Nash, Y. Charles Lu, Michael E. Anderson. 2009. Finite element modelling of

elastomeric sealing components for cylinder-head cover noise and vibration prediction. International Journal of vehicle design, Vol. 49, No.4, pp. 287-302

[4] Dennis R. Moss, Michael M. Basic. 2012. Pressure Vessel Design Manual. 4th Edition, Butterworth-Heinemann publication.

[5] James Walker Moorflex, 2005. 'Gasket technology guide', Understanding gaskets & dimensional guidebook, James Walker Moorflex Limited.

[6] M.F.Spotts, T.E.Shoup, 2011. Design of Machine Elements., Dorling Kindersley (India) Pvt .Ltd, 8th Edition, Licensees of Pearson Education.

[7] Catia V5, user manual.

[8] Ansys workbench 14.5, Ansys APDL 14.5, user manual.

[9] Koji Teramoto, Masahiko Anasoto, and Kazuaki Iwata. 1998. Coordinative Generation of Machining and Fixturing Plans by a Modularized Problem Solver. CIRP Annuals, Manufacturing Technology, Vol.47, pp. 437–440.

[10] Edgar R. Rodriguez Ramirez. 2012. The role of surprise on persuasion in industrial design. International Journal of Product Development, Vol.16, No.3/4, pp. 263 - 283.

[11] Bryan R. Fischer. 2011.GD&T Update Guide : ASME Y14.5-2009. Changes, Improvements, and Clarifications, Amer Society of Mechanical, Spi edition.

[12] G. Boothroyd and W. Knight. 1993. Manufacturing À La Carte : Efficiency : Design for assembly. IEEE Spectrum, pp.51-53

[13] DFMA, user manual.

[14] Geoffrey Boothroyd, Peter Dewhurst, Winston A. Knight, December 8, 2010. Third Edition. Product Design for Manufacture and Assembly. CRC Press Pages - 497 B/W Illustrations.

p-ISSN : 2335-1357 e-ISSN : 2437-1122

Mediterranean Journal of Modeling and Simulation

Med. J. Model. Simul. 05 (2016) 059-075

Bang-Bang Control Applied on an HIV-1 within host Model

A. Rahmoun [a] *, B. Ainseba [b] , D. Benmerzouk [a]

[a] Faculté des Sciences, Univ de Tlemcen, BP 119, Algerie.
[b] UMR CNRS 52 51, case 36 Univ Victor Segalan, Bordeaux2, 3ter place de la victoire, F 33067 Bordeaux cedex, France.

ARTICLE INFO

Article history :
Received March 2015
Accepted January 2016

Keywords :
HIV-1 ;
Mathematical model ;
Local controllability ;
Bang-bang control ;
Numerical simulations.

ABSTRACT

Local controllability analysis of an HIV infection model on which three controls are effective is investigated, the optimal control policy to minimize the number of infected cells, the number of free virus and maximize the number of healthy cells for each control separately, then for all controls applied at once is formulated and solved as an optimal bang-bang control problem (command all or nothing). Numerical examples are given to illustrate the obtained results.

1. Introduction

Treatment of patients infected by the Human Immunodeficiency Virus (HIV) is of great concern nowadays, aiming to find the optimal way for administering the cure.

Different chemotherapies are being tested, most widely using drugs as the reverse transcriptase inhibitors, integrase inhibitors or protease inhibitors, but clinical trials based on other forms of treatments are being performed, as the use of bee venom [3], antibodies [nature], the infusion of autologous $CD4^+$ T-cells in which the CCR5 gene was rendered permanently dysfunctional, (CCR5 is the major co receptor for human immunodeficiency virus) [4], injection of the Interleukin2 [8, 9], and so on.

HIV is an RNA virus, when it infects a human immune $CD4^+$ T-cell, its RNA is transcribed into DNA. Reverse transcriptase inhibitors interfere in this process by halting. the duplication of virus, consequently reducing the apoptosis phenomenon of the infected cells, integrase inhibitors can compromise the viral entry into the host cell which can seriously reduce the infection, on the other side the protease inhibitors interfere in the process of protein assembly of new viruses, which leads in the creation of non infectious

*Email : rahmoun_amel03@yahoo.fr

ones, easily cleared by immune cells, that helps in increasing clearance rate of virus.

Lot of data is available on the HIV-1 infection treatment, we know for example that many problems arise from the use of most chemotherapies with multiple and harmful side effects or ineffectiveness of treatment after a certain time due to the capability of the virus to mutate and become resistant, see [14] for example. For us, it is crucial to know if the application of multiple drugs is the best way of treatment, or if there is another way that can avoid or at least minimize side effects, while maintaining viral load under a specific threshold.

Motivated by this question, we have considered a system of Ordinary Differential Equations that describes the interaction of the immune system with the HIV-1, we have introduced treatments as three inputs to the model, we first study local controllability of the system for each control, then for all controls together, further, we consider objective functions to 1/ minimize infected cells, 2/ minimize free viruses in the blood, 3/ maximize healthy cells for each input separately, then for all inputs together at the same time, we derive the optimum strategy using the Pontryagin Maximum Principle, finally, numerical simulations are used to compare all cases.

In this paper we analyze the following system of Ordinary Differential Equations that models a cell-to-cell spread of HIV-1 infection in tissue culture based on the 3-Dimensional model considered by A. Perelson in [11], nevertheless, here, we consider the evolution of healthy cells as having a simple logistic growth, so our model is given by the following autonomous system :

$$\begin{cases} \dot{S}(t) = bS(t)(1 - \frac{S(t)}{K}) - \beta S(t)V(t) \\ \dot{I}(t) = -cI(t) + \beta S(t)V(t) \\ \dot{V}(t) = -dV(t) + rcI(t) \\ S(0) = S_0,\ I(0) = I_0,\ V(0) = V_0 \end{cases} \tag{S}$$

Where $S(\cdot)$ denotes the concentration of susceptible exposed (not yet infected) $CD4^+$ T-cells at time $t \in \Omega = [0, T]$; $I(\cdot)$ denotes the concentration of infectious $CD4^+$ T-cells and $V(\cdot)$ represents the concentration of free viruses at the same time. Put $x = (S, I, V)^T$ the vector of state variables.

b is the reproductive rate of healthy cells, K is the carrying capacity of the system, β is a constant rate at which a healthy cell meet a virus and becomes infected, also called the capturing rate, c, d are the clearance rates of infected cells and virus respectively ; r is the number of viruses released by an infected cell over its lifespan, sometimes called the conversion factor.

Initial conditions are fixed, we suppose $S_0 \leq K$ to fit reality, and all parameters of the system (S) are assumed to be strictly positive and are summarized in the following table :

Table 1 – Model's (S) parameters description.

Parameters	Significance	Value	Unit	References
b	Healthy cells reproduction rate	10	mm^3/day	[12]
K	Carrying capacity of the system	10^3	/ mm^3	Estimated
c	Death rate of infected cells	0.24	/ day	[12]
β	Rate of infection	2.4×10^{-5}	mm^3/day	[12]
d	Clearance rate of virions	2.4	/day	[13]
r	Number of virus released by an infected cell	3000	/day	[13]

2. Previous results

Proposition 1 [1]
The system (S) has three equilibriums :
– The origin,
– The infected-free (healthy) equilibrium, that we denote by $E_1 = (K, 0, 0)$,
– The chronic equilibrium, that we denote by $E^* = (S^*, I^*, V^*)$ where :

$$S^* = \frac{d}{r\beta},\ \ I^* = \frac{db}{cr\beta}(1 - \frac{d}{r\beta K}),\ \ V^* = \frac{b}{\beta}(1 - \frac{d}{r\beta K}).$$

This equilibrium only exists when the parameter $R_0 = \frac{r\beta K}{d}$ is greater than 1.
Proposition 2 [1]
– The positive octant is positively invariant by system (S), and all solutions of (S) are bounded.
– Local stability :
a) The origin is a saddle point
b) E_1 is locally asymptotically stable if $R_0 < 1$, locally stable but not asymptotically if $R_0 = 1$ and unstable if $R_0 > 1$.
c) E^* when it exists ($R_0 > 1$) is locally asymptotically stable if and only if $R > R_0 > 1$, where $R = \frac{2b(c+d)}{-\left[(c+d)^2+cd\right]+\sqrt{\left[(c+d)^2+cd\right]^2+4bcd(c+d)}}$.
– Global stability :
a) The healthy equilibrium $E_1 = (K, 0, 0)$ is Globally Asymptotically Stable if and only if $R_0 \leq 1$
b) When $R_0 > 1$ suppose the derivative of the logistic term in (S) is strictly negative for $S \in [0, K]$, then the chronic equilibrium point E^* is Globally Asymptotically Stable with respect to solutions not initiated on the S-axis.

3. Problem statement

We propose to control the model representing the HIV evolution with three inputs, one at each step, using controls $u_i(\cdot)$, $i = 1, 2, 3$, then apply all these controls at once.

a) The first one is applied on the virus directly to increase its clearance rate, it could be an antiretroviral drug like the so called Protease inhibitor (Pi) that has a direct effect of increasing the viral clearance, (see [10]), or it could be recent treatments like the use of nanoparticles carrying a toxin found in bee venom that are capable of destroying HIV particles while leaving neighboring cells intact, see [3], or some antibodies used to surround the virus in macrophage and keep it therein [2], or it could represent the association of all these treatments at the same time.

So, when therapy effects of the first control are taken into consideration, model reads as follows :

$$\begin{cases} \dot{S}(t) = bS(t)(1 - \frac{S(t)}{K}) - \beta S(t)V(t) \\ \dot{I}(t) = -cI(t) + \beta S(t)V(t) \\ \dot{V}(t) = -\overline{d}V(t) + rcI(t) \\ S(0) = S_0,\ I(0) = I_0,\ V(0) = V_0 \end{cases}$$

Where $\overline{d} = (1+\zeta_{Pi})d$, and ζ_{Pi} denotes the effectiveness of the administrated therapy in increasing natural death rate of virus, thus ζ_{Pi} may be considered as independent control input say u_1 which can be function of time t, one obtains then the first controlled system :

$$\dot{x}(t) = F_1(x(t),\, u_1(t)) \Leftrightarrow \begin{cases} \dot{S}\,(t) = bS(t)(1 - \frac{S(t)}{K}) - \beta S(t)V(t) \\ \dot{I}\,(t) = -cI(t) + \beta S(t)V(t) \\ \dot{V}\,(t) = -dV(t)(1 + u_1(t)) + rcI(t) \\ S(0) = S_0,\ I(0) = I_0,\ V(0) = V_0 \end{cases}$$

Characteristics of a sweetble function $u_1\,(\cdot)$ are to be defined further in the text.

b) The second control is employed to compromise the viral entry into the host cell, which is the first step of infection, so it will be applied on the term βSV in system (S), it could be the Integrase inhibitor or any entry inhibitor, it could be another type of treatment like the infusion of autologous $CD4^+$ T cells in which the CCR5 gene was rendered permanently dysfunctional[1] (see [4]), or it could be the regular use of microbicide gel that can block infection by the AIDS virus[2], as explained by the research in [5], it could be also the use of the CXCL4 protein, because its mechanism and its composition is totally different compared to all other proteins already known that regulate the movement of immune cells. CXCL4 protein directly binds to the virus, and is able to prevent HIV from entering human host cell [6], finely it could be the use of a compound of cannabis known to slow down the disease in advance states of AIDS [7].

Now model reads as follows :

$$\begin{cases} \dot{S}(t) = bS(t)(1 - \frac{S(t)}{K}) - \bar{\beta} S(t)V(t) \\ \dot{I}(t) = -cI(t) + \bar{\beta} S(t)V(t) \\ \dot{V}(t) = -dV(t) + rcI(t) \\ S(0) = S_0,\ I(0) = I_0,\ V(0) = V_0 \end{cases}$$

[1]CCR5 is the major co receptor for human immunodeficiency virus

[2]in experimentation for the human use, gave interesting results on simians

Where $\bar{\beta} = (1 - \zeta_{Ii})\beta$, ζ_{Ii} denotes the effectiveness of the therapy in decreasing the penetration of the virus in the CD4$^+$ cells and can be considered as an independent control, which leads us to our second controlled system

$$\dot{x}(t) = F_2(x(t),\, u_2(t)) \Leftrightarrow \begin{cases} \dot{S}(t) = bS(t)(1 - \frac{S(t)}{K}) - \beta S(t)V(t)(1 - u_2(t)) \\ \dot{I}(t) = -cI(t) + \beta S(t)V(t)(1 - u_2(t)) \\ \dot{V}(t) = -dV(t) + rcI(t) \\ S(0) = S_0,\, I(0) = I_0,\, V(0) = V_0 \end{cases}$$

c) The third control represents a manner to reduce the apoptosis of infected cells population, this will have as consequence to reduce the new born viruses, so, one wants to keep an infected cell alive as long as possible so that it doesn't release virions therein, it could be a treatment by the Reverse Transcriptase inhibitors, so it will be applied on the term $-cI$ in the system (S).

$$\begin{cases} \dot{S}(t) = bS(t)(1 - \frac{S(t)}{K}) - \beta S(t)V(t) \\ \dot{I}(t) = -\bar{c}I(t) + \beta S(t)V(t) \\ \dot{V}(t) = -dV(t) + r\bar{c}I(t) \\ S(0) = S_0,\, I(0) = I_0,\, V(0) = V_0 \end{cases}$$

Where $\bar{c} = (1 - \zeta_{RTI})c$, and ζ_{RTI} measures the effect of therapy in reducing the natural death rate of infected cells, that way one obtains the third controlled system

$$\dot{x}(t) = F_3(x(t),\, u_3(t)) \Leftrightarrow \begin{cases} \dot{S}(t) = bS(t)(1 - \frac{S(t)}{K}) - \beta S(t)V(t) \\ \dot{I}(t) = -cI(t)(1 - u_3(t)) + \beta S(t)V(t) \\ \dot{V}(t) = -dV(t) + rcI(t)(1 - u_3(t)) \\ S(0) = S_0,\, I(0) = I_0,\, V(0) = V_0 \end{cases}$$

d) When all controls applied at once, one has :

$$\dot{x}(t) = F(x(t),\, u_i(t)); i = 1,\, 2,\, 3 \Leftrightarrow \begin{cases} \dot{S}(t) = bS(t)(1 - \frac{S(t)}{K}) - \beta S(t)V(t)(1 - u_2(t)) \\ \dot{I}(t) = -cI(t)(1 - u_3(t)) + \beta S(t)V(t)(1 - u_2(t)) \\ \dot{V}(t) = -dV(t)(1 + u_1(t)) + rcI(t)(1 - u_3(t)) \\ S(0) = S_0,\, I(0) = I_0,\, V(0) = V_0 \end{cases}$$

Our goal is to study the model response to each of those controls separately, then see what happens when all of them are applied at once.

In fact, we have incorporated time dependent drug efficacies using controls $u_i(\cdot)$, $i = 1, 2, 3$. Note that setting $u_i(\cdot) = 0$ or $u_i(\cdot) = 1$, $i = 1, 2, 3$ in (S) would give either a non disease model or an uncontrolled model (i.e dynamics of the disease without treatment). Note also that values of $u_i > 1$, for $i = 2, 3$ correspond to treatment with a cytotoxic[3]

[3]Cytotoxicity is the quality of being toxic to cells. Examples of toxic agents are a chemical substance, an immune cell or some types of venom

drug, which is not the case of u_i, indeed this control is supposed to affect only virus particles, without having any effects on healthy or even infected cells, that is why its value is bounded by a constant L that might be larger than 1.

In view of this, consider the set :

$$U = \left\{ \begin{array}{l} u_i(t) \text{ is Lebesgue measurable } i = \overline{1,\,3}; a \leq u_1(t) \leq L, (L > 1)\ , \\ \text{and } 0 < a \leq u_i(t) \leq b < 1, \text{ for } i = 2,\,3,\, t \in [0,\,T] \end{array} \right\}$$

As the control admissible set.

4. Local controllability

Let's start with a study of local controllability of systems (S_i) , $i = \overline{1,\,3}$ and (S_c) at all equilibrium points :

Proposition 3 All systems are uncontrollable around the origin and the infection-free equilibrium, for any measurable bounded controls $u_i \in U$, $i = \overline{1,\,3}$.

Proof

Put :

$$A_1 = \frac{\partial F_1}{\partial x} = \begin{pmatrix} b(1-\frac{2S}{K}) - \beta V & 0 & -\beta S \\ \beta V & -c & \beta S \\ 0 & rc & -d(1+u_1) \end{pmatrix},\ B_1 = \frac{\partial F_1}{\partial u_1} = \begin{pmatrix} 0 \\ 0 \\ -dV \end{pmatrix}$$

$$A_2 = \frac{\partial F_2}{\partial x} = \begin{pmatrix} b(1-\frac{2S}{K}) - \beta V(1-u_2) & 0 & -\beta S(1-u_2) \\ \beta V(1-u_2) & -c & \beta S(1-u_2) \\ 0 & rc & -d \end{pmatrix},\ B_2 = \frac{\partial F_2}{\partial u_2} = \begin{pmatrix} \beta SV \\ -\beta SV \\ 0 \end{pmatrix}$$

$$A_3 = \frac{\partial F_3}{\partial x} = \begin{pmatrix} b(1-\frac{2S}{K}) - \beta V & 0 & -\beta S \\ \beta V & -c(1-u_3) & \beta S \\ 0 & rc(1-u_3) & -d \end{pmatrix},\ B_3 = \frac{\partial F_3}{\partial u_3} = \begin{pmatrix} 0 \\ cI \\ -rcI \end{pmatrix}$$

And

$$A_c = \frac{\partial F}{\partial x} = \begin{pmatrix} b(1-\frac{2S}{K}) - \beta V(1-u_2) & 0 & -\beta S(1-u_2) \\ \beta V(1-u_2) & -c(1-u_3) & \beta S(1-u_2) \\ 0 & rc(1-u_3) & -d(1+u_1) \end{pmatrix},$$

$$B_c = \frac{\partial F}{\partial u_i} = \begin{pmatrix} 0 & \beta SV & 0 \\ 0 & -\beta SV & cI \\ -dV & 0 & -rcI \end{pmatrix},\ i = 1,\,2,\,3$$

With the simple remark that $B_{1,2,3,c}|_{(0,0,0)} = B_{1,2,3,c}|_{(K,0,0)} = 0$, and using the Kalman criterion for local controllability [15], one concludes the result.

We now consider that $R_0 > 1$ and discuss the controllability around the chronic equilibrium E^*, in all systems :

Proposition 4 When $R_0 > 1$ all four systems $(S_1), (S_2), (S_3), (S_c)$ are locally controllable around E^*. If and only if R_0 is different from the values $\frac{2d}{d+c}$ and $\frac{2b}{b+c}$.

Proof

1) Case of system (S_1)

To simplify calculus put :

$$\begin{cases} X = b(1 - \frac{2S}{K}) \\ Y = \beta V \\ Z = \beta S \\ T = d(1 + u_1) \end{cases},$$

That way :

$$A_1 = \begin{pmatrix} X - Y & 0 & -Z \\ Y & -c & Z \\ 0 & rc & -T \end{pmatrix}$$

In this case, the Kalman matrix $\Lambda_1 = \begin{pmatrix} B_1 & A_1B_1 & A_1^2B_1 \end{pmatrix}$ is given by :

$$\Lambda_1 = -dV \begin{pmatrix} 0 & -Z & -Z(X - Y) + ZT \\ 0 & Z & -YZ - cZ - TZ \\ 1 & -T & rcZ + T^2 \end{pmatrix}$$

And

$$\det \Lambda_1 = -dVZ^2 \begin{vmatrix} -1 & -(X - Y) + T \\ 1 & -Y - c - T \end{vmatrix}$$

$$\det \Lambda_1 = -dVZ^2 [X + c]$$

$\det \Lambda_1$ vanishes for the quantity $X = -c$

Replacing in $X = b(1 - \frac{2S}{K})$ by S^* the first chronic equilibrium coordinate, one obtains :

If $R_0 \neq \frac{2b}{b+c}$ then $\det \Lambda_1 \neq 0$ and $rg\Lambda_1 = 3$ so, the system is locally controllable around the chronic equilibrium for any measurable bounded control $u_1 \in U$.

2) Case of system (S_2)

Here, to facilitate calculus, put :

$$\begin{cases} X = b(1 - \frac{2S}{K}) \\ Y = \beta V(1 - u_2) \\ Z = \beta S(1 - u_2) \end{cases},$$

That way :

$$A_2 = \begin{pmatrix} X-Y & 0 & -Z \\ Y & -c & Z \\ 0 & rc & -d \end{pmatrix}$$

In this case, the Kalman matrix $\Lambda_2 = \begin{pmatrix} B_2 & A_2B_2 & A_2^2B_2 \end{pmatrix}$ is

$$\Lambda_2 = \beta SV \begin{pmatrix} 1 & X-Y & (X-Y)^2 + rcZ \\ -1 & Y+c & Y(X-Y-c) - c(c+rZ) \\ 0 & -rc & rc(Y+c+d) \end{pmatrix}$$

And

$$\begin{aligned} \det \Lambda_2 = \; & rc\beta SV \left[(Y+c)(Y+c+d) + Y(X-Y-c) - c(c+rZ) + \right. \\ & \left. (X-Y)(Y+c+d) + (X-Y)^2 + rcZ\right] \end{aligned}$$

$$\det \Lambda_2 = rc\beta SV \left[(Y+c+d)(X+c) + Y(X-Y-c) - c^2 + (X-Y)^2\right]$$

This finely yields :

$$\det \Lambda_2 = rc\beta SV \left[X^2 + (c+d)X + dc\right]$$

So, $\det \Lambda_2$ vanishes for two values of X : $-c$ and $-d$.

Recall that $X = b\left(1 - \frac{2S}{K}\right)$, replacing by the chronic equibrium coordinates gives us two values of R_0 for which vanishes :

$$R_0 = \frac{2b}{b+c} \text{ and } R_0 = \frac{2d}{d+c}$$

So, if (and only if) $R_0 \neq \frac{2b}{b+c}$ and $R_0 \neq \frac{2d}{d+c}$ then $rg\Lambda_2 = 3$, hence the system is locally controllable around the chronic equilibrium for any measurable bounded control u_2.

3) Case of system (S_3)

To facilitate calculus, let's put :

$$\begin{cases} X = b(1 - \frac{2S}{K}) \\ Y = \beta V \\ Z = \beta S \\ \alpha = c(1-u_3) \end{cases} .,$$

A_3 reads as :

$$A_3 = \begin{pmatrix} X-Y & 0 & -Z \\ Y & -\alpha & Z \\ 0 & r\alpha & -d \end{pmatrix}$$

Here : $\Lambda_3 = \begin{pmatrix} B_3 & A_3B_3 & A_3^2B_3 \end{pmatrix}$
One gets :

$$\Lambda_3 = cI \begin{pmatrix} 0 & rZ & rZ(-\alpha + X - Y - d) \\ 1 & -\alpha - rZ & \alpha^2 + r\alpha Z + rZ(Y + \alpha + d) \\ -r & r(\alpha + d) & -r\left[\alpha^2 + d\alpha + (rZ\alpha + d^2)\right] \end{pmatrix}$$

And

$$\det \Lambda_3 = cr^2 IZ \begin{vmatrix} 0 & 1 & -\alpha + X - Y - d \\ 1 & -\alpha - rZ & \alpha^2 + r\alpha Z + rZ(Y + \alpha + d) \\ -1 & \alpha + d & -\left[\alpha^2 + d\alpha + (rZ\alpha + d^2)\right] \end{vmatrix}$$

Basic calculus yields :

$$\det \Lambda_3 = cr^2 IZ \left[X\left(d - rZ\right) - Yd\right]$$

When replacing by the chronic equilibrium coordinates, one gets that $(d - rZ) = 0$ so :

$$\det \Lambda_3 = -\frac{b^2}{\beta} d^3 \left(1 - \frac{1}{R_0}\right)^2$$

In this case, the system (S_3) is locally controllable around the chronic equilibrium for any measurable bounded control u_3.
4) Case of system (S_c)
Recall that

$$B_c = \begin{pmatrix} 0 & \beta SV & 0 \\ 0 & -\beta SV & cI \\ -dV & 0 & -rcI \end{pmatrix}$$

In this case,

$$\det B_c = -dV(c\beta SVI) \neq 0$$

So the Kalman matrix $\Lambda = \begin{pmatrix} B_c & A_cB_c & A_c^2B_c \end{pmatrix}$ is of $rank = 3$. This means that the system (S_c) is also locally controllable around the chronic equilibrium for all measurable bounded controls u_i, $i = 1, 2, 3$.

In view of those results, all our systems (S_i), $i = 1, 2, 3, c$, are locally controllable around E^* if and only if R_0 is different from the two values in the set : $\left\{\frac{2d}{d+c}, \frac{2b}{b+c}\right\}$.

5. Optimal control

– Case of system (S_1)

We want to minimize the number of infected cells in the body, so consider the cost function :

$$J_I\left[u_1\right] = \min_{u_1 \in U} \int_0^T I(t)dt.$$

Using the Pontryaguin Maximum Principle (see [15]) to compute the optimal control one has the Hamiltonian of the system (S_1) as follows :

$$\begin{aligned} H(t,\, x,\, \lambda,\, u_1) = \quad & -I(t) + \lambda_1(t)\left(bS(t)(1-\tfrac{S(t)}{K}) - \beta S(t)V(t)\right) + \\ & \lambda_2(t)\left(-cI(t) + \beta S(t)V(t)\right) + \lambda_3(t)\left(-dV(t)(1+u_1(t)) + rcI(t)\right) \end{aligned}$$

And the corresponding adjoint equations :

$$\begin{cases} \dot{\lambda}_1(t) = -\frac{\partial H}{\partial S} = -\lambda_1(t)\left[b(1-\frac{2S(t)}{K}) - \beta V(t)\right] - \lambda_2(t)\beta V(t) \\ \dot{\lambda}_2(t) = -\frac{\partial H}{\partial I} = 1 + c\lambda_2(t) - rc\lambda_3(t) \\ \dot{\lambda}_3(t) = -\frac{\partial H}{\partial V} = \beta S(t)\lambda_1(t) - \beta S(t)\lambda_2(t) + d(1+u_1(t))\lambda_3(t) \\ \lambda_1(T) = \lambda_2(T) = \lambda_3(T) = 0 \text{ are the transversality conditions} \end{cases}$$

The control u_1^* is optimal if it verifies the maximum principle :

$$H(t,\, x,\, \lambda,\, u_1^*) = \max_{u_1 \in U} H(t,\, x,\, \lambda,\, u_1).$$

The Hamiltonian being linear in the control, the optimal policy will be a combination between bang-bang control and singular control.

The Pontryaguin Maximum Principle leads to :

$$-dV(t)\lambda_3(t)u_1^*(t) = \max_{u_1 \in U} -dV(t)\lambda_3(t)u_1(t)$$

Put $\varphi\left(t\right) = -dV\left(t\right)\lambda_3\left(t\right)$ the switch function; recall that moments of switch are the zeros of function φ.

We get to the characterization of our optimal bang-bang control :

$$u_1^*(t) = \begin{cases} u_{\min} \text{ if } \phi(t) < 0 \\ u_{\max} \text{ if } \phi(t) > 0 \\ \text{undefined if } \phi(t) = 0 \end{cases}$$

d and V being always strictly positive, one has :

$$u_1^*(t) = \begin{cases} a \text{ if } \lambda_3(t) > 0 \\ L \text{ if } \lambda_3(t) < 0 \\ \text{undefined if } \lambda_3(t) = 0 \end{cases}$$

Taking a look in the derivative of φ, and considering that $\varphi(T) = \lambda_3(T) = 0$ one concludes that $\frac{\partial \varphi}{\partial t}$ vanishes for at most one $t^* \in \mathring{\Omega}$ and hence φ changes its sign at most once on Ω. So there is no singular control and the optimal control reduces to the bang-bang one.

Using the same method, one obtains the bang-bang optimal control for minimizing the level of free viruses in the blood using the cost function : $J_V[u_1] = \min_{u_1 \in U} \int_0^T V(t)dt$, and maximizing healthy cells using the cost function : $J_V[u_1] = \min_{u_1 \in U} \int_0^T V(t)dt$ in (S_1) the expression of the optimal control is unchanged, only expressions of the associated Hamiltonians and corresponding adjoint systems change, we omit them here for convenience.

– Case of system (S_2) and (S_3)

For the remaining systems, by the same way, we derive the expressions of the optimal bang-bang controls, summarized in what follows :

$$u_2^*(t) = \begin{cases} a \text{ if } \lambda_2(t) - \lambda_1(t) < 0 \\ b \text{ if } \lambda_2(t) - \lambda_1(t) > 0 \\ \text{undefined if } \lambda_2(t) - \lambda_1(t) = 0 \end{cases}$$

Here, we can use the fact that $\frac{\partial^2 H}{\partial u_2^2} = 0$ (the Hamiltonian being linear in the control) to conclude that there is no singular control.

$$u_3^*(t) = \begin{cases} a \text{ if } r\lambda_3(t) - \lambda_2(t) < 0 \\ b \text{ if } r\lambda_3(t) - \lambda_2(t) > 0 \\ \text{undefined if } r\lambda_3(t) - \lambda_2(t) = 0 \end{cases}$$

Again, one obtains the same expressions of u_2^*, and u_3^* when minimizing the level of free viruses and maximizing healthy cells in (S_2), and (S_3) respectively, notice that expressions of Hamiltonians and adjoint systems change depending on the associate case, we omit them here to avoid repetition.

– Case of system (S_c)

The Hamiltonian associated with system (S_c) is :

$$\begin{aligned} H(t, X, \lambda, u_c) = \; & L(t) + \lambda_1(t)\left[bS(t)\left(1 - \tfrac{S(t)}{K}\right) - \beta S(t)V(t)(1 - u_2(t))\right] \\ & + \lambda_2(t)\left[-cI(t)(1 - u_3(t)) + \beta S(t)V(t)(1 - u_2(t))\right] \\ & + \lambda_3(t)\left[rcI(t)(1 - u_3(t) - dV(t)(1 + u_1(t))\right] \end{aligned}$$

Where $L(t)$ represents the objective functional to optimize, i.e :

$$L(t) = \begin{cases} -I(t) \text{ when minimizing the infected cells population} \\ -V(t) \text{ when minimizing the virus particles number} \\ S(t) \text{ when maximizing the healthy cells population} \end{cases}$$

The associated adjoint system when minimizing infected cells population is :

$$(S'_{Ic}) \begin{cases} \dot{\lambda}_1(t) = -\frac{\partial H}{\partial S} = \left[\beta V(t)(1-u_2(t)) - b\left(1-\frac{2S(t)}{K}\right)\right]\lambda_1(t) - \\ \qquad [\beta V(t)(1-u_2(t))]\,\lambda_2(t) \\ \dot{\lambda}_2(t) = -\frac{\partial H}{\partial I} = [c(1-u_3(t))]\,\lambda_2(t) - [rc(1-u_3(t))]\,\lambda_3(t) + 1 \\ \dot{\lambda}_3(t) = -\frac{\partial H}{\partial V} = [\beta S(t)(1-u_2(t))]\,\lambda_1(t) - [\beta S(t)(1-u_2(t))]\,\lambda_2(t) + \\ \qquad [d(1+u_1(t))]\,\lambda_3(t) \\ \lambda_1(T) = \lambda_2(T) = \lambda_3(T) = 0 \text{ are the transversality conditions} \end{cases}$$

Whereas when minimizing the virus particles number, the associated adjoint system is :

$$(S'_{Vc}) \begin{cases} \dot{\lambda}_1(t) = -\frac{\partial H}{\partial S} = \left[\beta V(1-u_2(t)) - b\left(1-\frac{2S(t)}{K}\right)\right]\lambda_1(t) - \\ \qquad [\beta V(t)(1-u_2(t))]\,\lambda_2(t) \\ \dot{\lambda}_2(t) = -\frac{\partial H}{\partial I} = [c(1-u_3(t))]\,\lambda_2(t) - [rc(1-u_3(t))]\,\lambda_3(t) \\ \dot{\lambda}_3(t) = -\frac{\partial H}{\partial V} = [\beta S(t)(1-u_2(t))]\,\lambda_1(t) - [\beta S(t)(1-u_2(t))]\,\lambda_2(t) + \\ \qquad [d(1+u_1(t))]\,\lambda_3(t) + 1 \\ \lambda_1(T) = \lambda_2(T) = \lambda_3(T) = 0 \text{ are the transversality conditions} \end{cases}$$

And, when maximizing the healthy cells populations, one gets :

$$(S'_{Sc}) \begin{cases} \dot{\lambda}_1(t) = -\frac{\partial H}{\partial S} = \left[\beta V(1-u_2(t)) - b\left(1-\frac{2S(t)}{K}\right)\right]\lambda_1(t) - \\ \qquad [\beta V(t)(1-u_2(t))]\,\lambda_2(t) - 1 \\ \dot{\lambda}_2(t) = -\frac{\partial H}{\partial I} = [c(1-u_3(t))]\,\lambda_2(t) - [rc(1-u_3(t))]\,\lambda_3(t) \\ \dot{\lambda}_3(t) = -\frac{\partial H}{\partial V} = [\beta S(t)(1-u_2(t))]\,\lambda_1(t) - [\beta S(t)(1-u_2(t))]\,\lambda_2(t) + \\ \qquad [d(1+u_1(t))]\,\lambda_3(t) \\ \lambda_1(T) = \lambda_2(T) = \lambda_3(T) = 0 \text{ are the transversality conditions} \end{cases}$$

By the Pontryagin Maximum Principle to compute the optimal control, one gets :

$$u_1^*(t) = \begin{cases} a \text{ if } \lambda_3(t) > 0 \\ L \text{ if } \lambda_3(t) < 0 \\ \text{undefined if } \lambda_3(t) = 0 \end{cases}$$

$$u_2^*(t) = \begin{cases} a \text{ if } \lambda_2(t) - \lambda_1(t) < 0 \\ b \text{ if } \lambda_2(t) - \lambda_1(t) > 0 \\ \text{undefined if } \lambda_2(t) - \lambda_1(t) = 0 \end{cases}$$

$$u_3^*(t) = \begin{cases} a \text{ if } r\lambda_3(t) - \lambda_2(t) < 0 \\ b \text{ if } r\lambda_3(t) - \lambda_2(t) > 0 \\ \text{undefined if } r\lambda_3(t) - \lambda_2(t) = 0 \end{cases}$$

6. Numerical simulations

6.1. The uncontrolled system

We begin by simulate the system without any control input to visualize its behavior, and we distinguish three cases depending on the parameter R_0, as resumed in propositions 1, initial conditions are considered as $S_0 = 1000$, $I_0 = 10$, $V_0 = 100$ [estimated], $T = 400$:

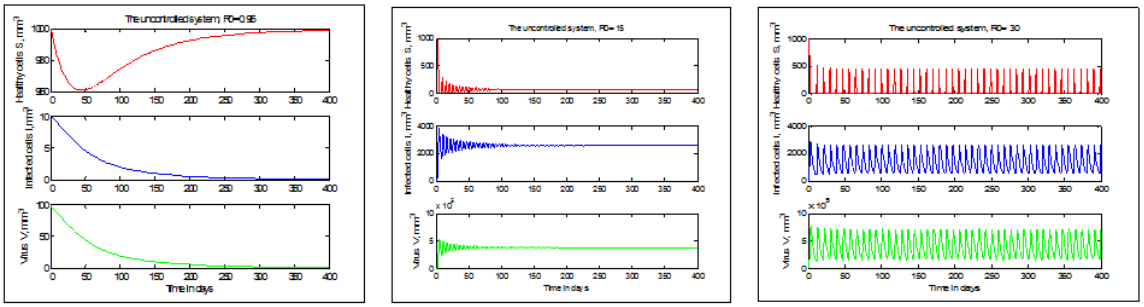

(a) (b) (c)

Fig. 1 – The uncontrolled system (S).

Fig. 1 shows :

- In (a) the dynamics of healthy and infected cells, as well as free virus in the uncontrolled model (S) with $R_0 = 0.96 < 1$, one sees clearly that the infection dies out. Here the parameters chosen were : $d = 5$, $c = 0.24$, $\beta = 0.000024$, $b = 0.03$, $r = 200$, $K = 1000$.
- In (b), global stability when using the parameters $d = 5$, $c = 0.24$, $\beta = 0.000024$, $b = 0.03$, $r = 1500$, $K = 1000$ to get $1 < (R_0 = 15) < (R = 15.90)$
- In (c) a periodic solution when using parameters of table 1 in the uncontrolled model (S) ; here : $(R_0 = 30) > (R = 15.90) > 1$.

6.2. The controlled system

Now, we discuss the numerical solutions of the optimality system and the corresponding optimal controls, and give interpretations for various cases.

Figures are obtained by solving the optimality system consisting of 6 ODEs from the state and the corresponding adjoint equations. An iterative method is used for solving the optimality system. We start by solving the state equations with a guess for the control over the simulated time using a forward (because of initial state conditions) fourth order Runge-Kutta scheme, followed by a backward (because of the final adjoint conditions) implicit Euler scheme for the adjoint equations and using the current iteration solution of the state equations. Then the controls are updated from the characterization (1). This process is repeated and iterations are stopped if the values of unknowns at the previous iteration are very close to the ones at present iteration.

Parameters of table 1 were used, Initial conditions are considered as $S_0 = 1000$, $I_0 = 10$, $V_0 = 100$ [estimated], $T = 50$, final adjoint variables are zero in all cases, parameters used were : $a = 0.01$ and $b = 0.9$, $L = 5$ [estimated] in all cases.

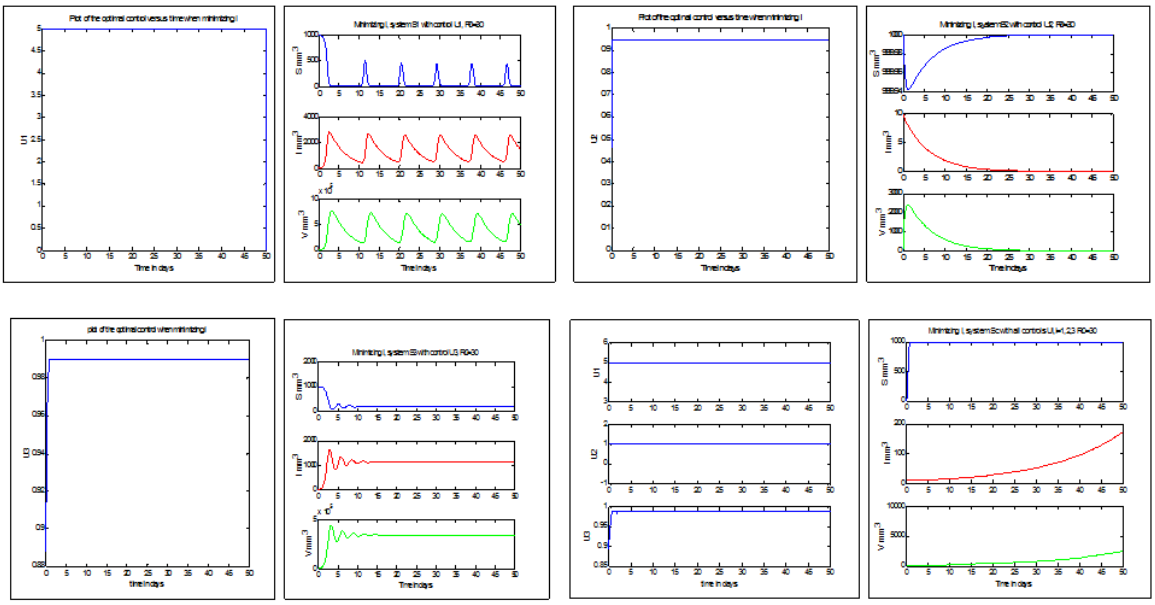

Fig. 2 – The controlled system (S_i) when minimizing infected cells population, $i = 1, 2, 3, c$.

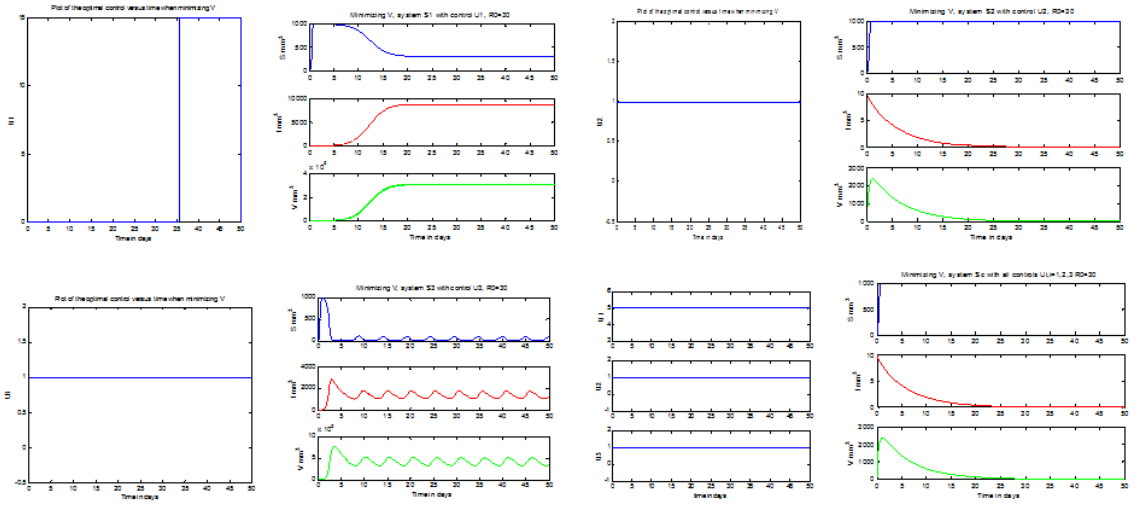

Fig. 3 – The controlled system (S_i) when minimizing virus population, $i = 1, 2, 3, c$.

Fig. 2. shows on the left hand side the plot of optimal controls $u_i, i = \overline{1,3}$, as function of time, and on the right hand side the corresponding densities of healthy and infected cells as well as free viruses circulating in the blood in the associated controlled system when minimizing the infected cells population (When u_i is active, then $u_j = 0$ for $j \neq i$, $i, j = \overline{1,3}$).

Despite the fact that the first control is always in its maximal value, and reduces efficiently the number of infected cells, it is not very effective on the overall infection ; this

might be due to the fact that the number of new born viruses still is much greater than the modified clearance rate.

On the other hand, the second control, which is also always in its maximum value, is very effective and has an instantaneous effect in turning over the viruses as well as infected cells, and driving the healthy cells to the top value.

The third control is in its maximal value, and is very effective in reducing the number of infected cells as wanted, after this, healthy cells gets stabilized in a low level and viruses in a relatively high level, that is why this control is considered not to be very effective.

When all controls are applied together, infection is well controlled, certainly thanks to the second control more than any other one.

Figure 3 shows on the left hand side the plot of optimal controls $u_i, i = \overline{1,3}$, as function of time, and on the right hand side the corresponding densities of healthy and infected cells as well as free viruses circulating in the blood in the associated controlled system when minimizing the virus population (When u_i is active, then $u_j = 0$ for $j \neq i, i, j = \overline{1,3}$)

The first control is on its minimal value until day 35 when it jumps to its maximal value. It is quite effective in reducing the number of free viruses that stabilizes around $3 \times 10^5 mm^3$ the overall infection, wherever, is derived to a point where healthy cells get stabilized in a quite low level and infected cells as well as viruses get stabilized in a high level.

Once again, control u_2 is very effective, but control u_3 here gives very bad results in comparison with the "minimizing infected cells" case, because oscillations occur driving healthy cells to a minimal threshold and infected as well as viruses to a higher level, the increase of infected cells can be a consequence of the cellular division also, not only a direct effect on infection ; that is why u_3 can be considered as "not very effective".

Finely, using all controls together is very effective.

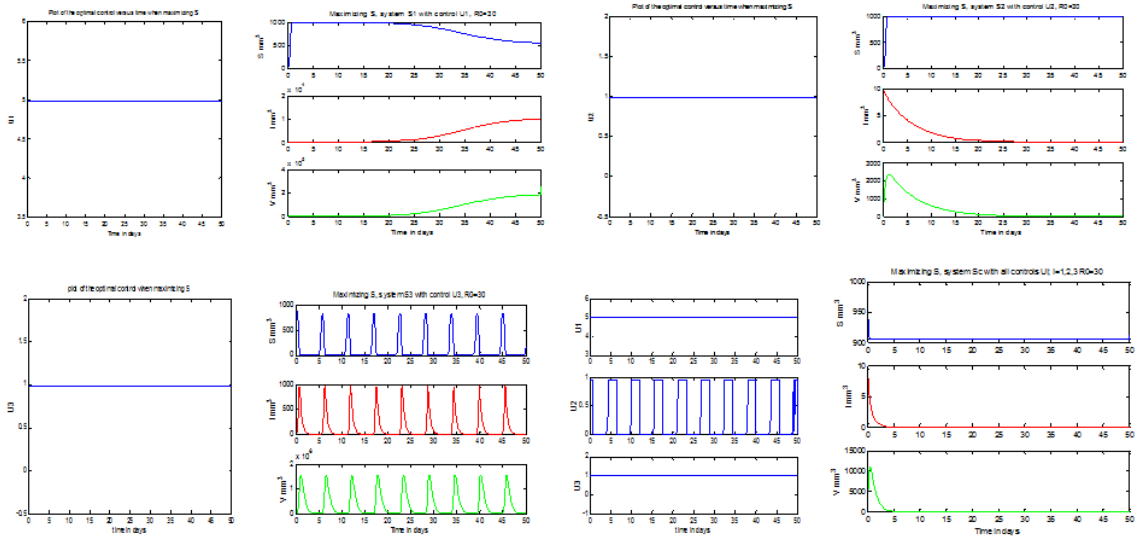

Fig. 4 – The controlled system (S_i) when maximizing healthy cells population, $i = 1, 2, 3, c$.

Figure 4 shows on the left hand side the plot of optimal controls $u_i, i = \overline{1,3}$ as function of time, and on the right hand side the corresponding densities of healthy and infected cells as well as free viruses circulating in the blood in the associated controlled system when maximizing healthy cells population (When u_i is active, then $u_j = 0$ for $j \neq i$, $i, j = \overline{1,3}$)

When maximizing healthy cells, control u_1 works pretty well and keeps the infection away until day 30, where one can notice a decline in healthy cells population and an instantaneous increase in infected cells and virus population driving the infection to move forward.

Control u_2 is very effective as usual, but control u_3 seems to be absolutely not effective, even if the number of infected cells and free virus are reduced, the oscillations occur which precludes that the infection is not controlled.

When all controls are effective, the infection is once again well controlled.

7. Conclusion

A mathematical model that deals with the spread of infection by the Human Immunodeficiency Virus of type one (HIV-1) in vivo in which the evolution of healthy cells has a logistic growth was considered, local controllability was studied and the optimal bang-bang policy using the Pontryagin Maximum Principle was performed to achieve three goals : firstly to minimize the number of infected cells into the body, secondly to minimize the number of free virus particles circulating in the blood and finely, to maximize the number of healthy $CD4^+$ T-cells. This was done using three decoupled controls. After this, those controls were applied at once on the system. Numerical simulations were given to compare all cases.

Our comparative study on the controls is of great importance, knowing that adherence to the "Highly Active Antiretroviral Therapy" (HAART) is a significant problem, many patients have troubles with the dosing requirement, in addition, side effects of such therapies can be severe ; a regimen that could reduce dosage requirements or the drugs taken while maintaining control over viral plasma levels might not only increase patient adherence but also the overall health of the patient by reducing side effects.

According to these simulations, it comes that u_2, the control applied to compromise the viral entry to the cell is the "best" way to 1/minimize infected cells population, 2/ maximize healthy cells population, and even 3/ minimize free circulating virus ; it is now a real question for scientists to know if the use of other controls really decreases the overall infection in a significant manner, or if it only increases treatment resistance and side effects. Balance between the use of different treatments and clinical situation of the concerned infected being has to be found.

REFERENCES

[1] A. Rahmoun, D. Benmerzouk and B. Ainseba, “Bifurcation analysis of the HIV-1 within host model”, Mathematical Methods in the Applied Sciences, DOI : 10.1002/mma.3609, (2015).

[2] Stefano Berre, Raphaël Gaudin, and al "CD36-specific antibodies block release of HIV-

1 from infected primary macrophages and its transmission to T cells", The Journal of Experimental Medicine, (2013) Vol. 210 No. 122523-2538

[3] Joshua L Hood, Andrew P Jallouk, Nancy Campbell, Lee Ratner, Samuel A Wickline, "Cytolytic nanoparticles attenuate HIV-1 infectivity", Antiviral Therapy 2013 ;18 :95–103 (doi : 10.3851/IMP2346)

[4] Pablo Tebas, M.D., David Stein, M.D., Winson W. Tang, M.D., Ian Frank, M.D., Shelley Q. Wang, M.D., Gary Lee, Ph.D., S. Kaye Spratt, and al "Gene Editing of CCR5 in Autologous CD4 T Cells of Persons Infected with HIV" The New England Journal of Medicine, 370 :901-910March 6, 2014DOI : 10.1056/NEJMoa1300662.

[5] Nathalie Dereuddre-Bosquet, Laurence Morellato-Castillo, Joachim Brouwers, and al "MiniCD4 Microbicide Prevents HIV Infection of Human Mucosal Explants and Vaginal Transmission of SHIV162P3 in Cynomolgus Macaques ",DOI : 10.1371/journal.ppat.1003071(2012).

[6] DJ Auerbach et al., Identification of the platelet-derived chemokine CXCL4/PF-4 as a broad-spectrum HIV-1 inhibitor. Proceeding of the National Academy of Sciences of the United States of America DOI : 10.1073/pnas.1207314109 (2012).

[7] Cristina Maria Costantino, Achla Gupta, Alice W. Yewdall, Benjamin M. Dale, "Cannabinoid Receptor 2-Mediated Attenuation of CXCR4-tropic HIV Infection in Primary CD4 + T Cells" PLoS ONE published March 20, 2012 10.1371/journal.pone.0033961

[8] Christopher S. Henney, Kagemasa Kuribayashi, Donald E. Kern and Steven Gillis, "Interleukin-2 augments natural killer cell activity", Nature 291, 335 - 338 (28 May 1981) ; doi :10.1038/291335a0

[9] L. Mollet, B. Autran, "Lymphocytes T cytotoxiques spécifiques du virus de l'immunodéficience humaine", Virologie. Volume 5, Numéro 1, 23-34, Janvier - Février 2001.

[10] M-J. Mhawej, C. H. Moog, F. Biafore, C. Brunet-François, "control of the HIV infection and drug dosage" Biomedical Signal Processing and Control, vol. 5, pp. 45-52, 2010.

[11] A. Perelson and P. Nelson, "mathematical analysis of HIV-1 Dynamics in vivo", SIAM Review, vol. 41, no. 1, pp. 3-44, 1999.

[12] K. R. Fister, S. Lenhart, J .S . McNally, "Optimizing Chemotherapy in an HIV Model", Electronic Journal of Differential Equations, vol. 32, no. 1. 1998.

[13] D. E. Kirschner, F. Webb, M. Cloyd, Model of HIV-1 Disease Progression Based on Virus-Induced Lymph Node Homing and Homing-Induced Apoptosis of CD4+ Lymphocytes, Journal of Acquired Immune Deficiency Syndromes, vol. 24, pp. 352-362, 2000.

[14] Libin Rong, Zhilan Feng, Alan S. Perelson, " Emergence of HIV-1 Drug Resistance During Retroviral Treatment", Bulletin of Mathematical Biology (2007) 69 :2027-2060.

[15] E.Trélat, "Contrôle Optimal : Théorie et applications", Laboratoire AN-EDP, Université Paris-sud.